A transcription factor binding atlas for photosynthesis in cereals identifies a key role for coding sequence in the regulation of gene expression

Steven J. Burgess[*1], Ivan Reyna-Llorens[*1], Katja Jaeger[2] and Julian M. Hibberd[1]

[1]Department of Plant Sciences, Downing Street, University of Cambridge, Cambridge CB2 3EA, UK.

[2]Sainsbury Laboratory, University of Cambridge, 47 Bateman Street, Cambridge, CB2 1LR, UK.

I-RL - suallorens@gmail.com

SJB - sjb287@cam.ac.uk

KJ - katja.jaeger@slcu.cam.ac.uk

JMH (corresponding) - jmh65@cam.ac.uk. Tel - +44(0) 1223 766547

[*]These authors contributed equally to this work

Keywords: Photosynthesis, gene regulation, evolution, cereals, transcription factor binding sites

Summary

The gene regulatory architecture associated with photosynthesis is poorly understood. Most plants use the ancestral C_3 pathway, but our most productive cereal crops use C_4 photosynthesis. In these C_4 cereals, large-scale alterations to gene expression allow photosynthesis to be partitioned between cell types of the leaf. Here we provide a genome-wide transcription factor binding atlas for grasses that operate either C_3 or C_4 photosynthesis. Most of the >950,000 sites bound by transcription factors are preferentially located in genic sequence rather than promoter regions, and specific families of transcription factors preferentially bind coding sequence. Cell specific patterning of gene expression in C_4 leaves is associated with combinatorial modifications to transcription factor binding despite broadly similar patterns of DNA accessibility between cell types. A small number of DNA motifs bound by transcription factors are conserved across 60 million years of grass evolution, and C_4 evolution has repeatedly co-opted at least one of these hyper-conserved *cis*-elements. The grass cistrome is highly divergent from that of the model plant *Arabidopsis thaliana*.

Introduction

Photosynthesis sets maximum crop yield, but despite millions of years of natural selection is not optimised for either current atmospheric conditions or agricultural practices (Long et al., 2015; Ort et al., 2015). The majority of photosynthetic organisms, including crops of global importance such as wheat, rice and potato use the C_3 photosynthesis pathway in which Ribulose-Bisphosphate Carboxylase Oxygenase (RuBisCO) catalyses the primary fixation of CO_2. However, carboxylation by RuBisCO is competitively inhibited by oxygen binding the active site (Bowes et al., 1971). This oxygenation reaction generates toxic waste-products that are recycled by an energy-demanding series of metabolic reactions known as photorespiration (Bauwe et al., 2010; Tolbert, 1971). The ratio of oxygenation to carboxylation increases with temperature (Jordan and Ogren, 1984; Sharwood et al., 2016) and so losses from photorespiration are particularly high in the tropics. When oxygenation is reduced through CO_2 enrichment, crops show increased photosynthetic efficiency and higher yields (Leakey et al., 2012). In addition to the inefficiency associated with oxygenation by RuBisCO, due to the rapid rise in atmospheric CO_2 concentrations from ~220 to 400ppm, the stoichiometry and kinetics of other photosynthesis enzymes are considered sub-optimal. For example, increased activity of Sedoheptulose 1,7-bisphosphatase improves photosynthesis and yield (Lefebvre et al., 2005; Miyagawa et al., 2001). Furthermore, the ability of leaves to harness light and generate chemical energy is neither optimised for current crop canopy structures (Zhu et al., 2010b) or rapid fluctuations in light (Kromdijk et al., 2016). Thus, although it is clear that improving C_3 photosynthesis would drive increased crop yields, we have an incomplete understanding of the genes that underpin this fundamental process.

The inefficiencies associated with C_3 photosynthesis in the tropics have led to multiple plant lineages evolving mechanisms that suppress oxygenation by concentrating CO_2 around RuBisCO. One such evolutionary strategy is known as C_4 photosynthesis. Species that use the C_4 pathway include maize, sorghum and sugarcane, and they represent the most productive crops on the planet (Sage and Zhu, 2011). In C_4 leaves, additional expenditure of ATP, alterations to leaf anatomy and cellular ultrastructure, as well as spatial separation of photosynthesis between compartments (Hatch, 1987) allows CO_2 concentration to be increased around tenfold compared with that in the atmosphere (Furbank, 2011). Despite the complexity of C_4 photosynthesis, it is

73 found in over 60 independent plant lineages and so represents one of the most remarkable
74 examples of convergent evolution known to biology (Sage et al., 2011). In most C_4 plants the initial
75 RuBisCO-independent fixation of CO_2 and the subsequent RuBisCO-dependent reactions take
76 place in distinct cell-types known as mesophyll and bundle sheath cells, and so are associated with
77 strict patterning of gene expression between these cell-types. Although the spatial patterning of
78 gene expression is fundamental to C_4 photosynthesis, very few examples of *cis*-elements or *trans*-
79 factors that generate cell-preferential expression required for C_4 photosynthesis have been
80 identified (Brown et al., 2011; Gowik et al., 2004; Williams et al., 2016). In summary, in both C_3 and
81 C_4 species, work has focussed on analysis of mechanisms controlling the expression of individual
82 genes, and so our understanding of the overall landscape associated with photosynthesis gene
83 expression is poor.

84 In yeast and animal systems, the high sensitivity of open chromatin to DNase-I (Zentner and
85 Henikoff, 2014) has allowed comprehensive, genome-wide characterisation of transcription factor
86 binding sites at single nucleotide resolution (Hesselberth et al., 2009; Neph et al., 2012; Thurman
87 et al., 2012). Despite the power of this approach to define regulatory DNA and the likely
88 transcription factors binding these sequences, this approach has not yet been used to provide
89 insight into the regulatory architecture of photosynthetic leaves of major crops except rice (Zhang
90 et al., 2012b). Moreover, although leaves are composed of multiple distinct cell-types, differences
91 in transcription factor binding between cells have not yet been assessed in plants. By carrying out
92 DNase I-SEQ on grasses that use either C_3 or C_4 photosynthesis, we provide comprehensive
93 insight into the transcription factor binding repertoire associated with each form of photosynthesis.
94 The data indicate that specific cell types from leaf tissue make use of a markedly distinct *cis*-
95 regulatory code, and that transcription factor binding is more frequent within genes than promoter
96 regions. Despite significant conservation in the transcription factors families binding DNA in
97 grasses, it is also apparent that the binding sites they recognise are subject to high rates of
98 mutation. Comparison of sites bound by transcription factors in both C_3 and C_4 leaves
99 demonstrates that the repeated evolution of C_4 photosynthesis is built on combination of *de novo*
100 gain of *cis*-elements and exaptation of highly conserved regulatory elements found in the ancestral
101 C_3 system.

102 **Results**

103 **A *cis*-regulatory atlas for monocotyledons**

104 Four grass species were selected to provide insight into the regulatory architecture associated
105 with C_3 and C_4 photosynthesis. *Brachypodium distachyon* uses the ancestral C_3 pathway (Figure
106 1A). *Sorghum bicolor, Zea mays* and *Setaria italica* all use C_4 photosynthesis although
107 phylogenetic reconstructions indicate that *S. italica* represents an independent evolutionary origin
108 of the C_4 pathway (Figure 1A). Nuclei from leaves of *S. italica* (C_4), *S. bicolor* (C_4), *Z. mays* (C_4)
109 and *B. distachyon* (C_3) were treated with DNase I (Figure S1) and subjected to deep sequencing. A
110 total of 799,135,794 reads could be mapped to the respective genome sequences of these species
111 (Table S1). 159,396 DNase-hypersensitive sites (DHS) of between 150-15,060 base pairs
112 representing broad regulatory regions accessible to transcription factor binding were identified from
113 all four genomes (Figure 1B). Between 20,817 and 27,746 genes were annotated as containing at
114 least one DHS (Table S2). Within these DHS, 533,409 digital genomic footprints (DGF)
115 corresponding to individual transcription factor binding sites of between 11 and 25 base pairs were
116 identified through differential accumulation of reads mapping to positive or negative strands around
117 transcription factor binding sites (Figure 1B&C). At least one transcription factor footprint was
118 identified in >75% of the broader regions defined by DHS (Table S2). In contrast to the preferential
119 binding of transcription factors to AT-rich DNA observed in *A. thaliana* all four grasses DGF had a
120 greater GC content compared with the genome average (Table S3).

121 DHS and DGF were primarily located in gene-rich regions, and depleted around centromeres
122 (Figure 1D). Individual transcription factor binding sequences were resolved in all chromosomes
123 from each species (Figure 1D). Many genes contained DGF that have previously been associated
124 with specific classes of transcription factors. For example, the *SbPPC* gene (Sobic.010G160700)
125 encoding phospho*enol*pyruvate carboxylase that catalyses the first committed step of C_4
126 photosynthesis, contained sixteen DGF of which six are associated with known transcription factor
127 families (Figure 1D). On a genome-wide basis, the distribution of DGF was similar between
128 species, with the highest proportion of such sites located in promoter, coding sequence (CDS) and
129 intergenic regions (Figure 1E). However, when normalised to the length of such regions, the
130 density of transcription factor recognition sites was highest in 5' untranslated regions (UTRs),

131 coding sequences (CDS) and 3' UTRs (Figure 1F). In all four species promoter regions contained
132 fewer DGF than genic sequence (Figure 1F) and distribution plots showed that the density of DGF
133 was highest in exonic sequences downstream of the annotated transcriptional start sites (Figure
134 S2).
135

136 **A distinct *cis*-regulatory lexicon for specific cells within the leaf**

137 The above analysis provides a genome-wide overview of the *cis*-regulatory architecture
138 associated with photosynthesis in leaves of grasses. However, as with other complex multicellular
139 systems, leaves are composed of many specialised cell types. Because each DGF is defined by
140 fewer sequencing reads mapping to the genome compared with the larger DHS region, depleted
141 signals derived from low abundance cell-types cannot be detected from such tissue-level analysis
142 (Figure 2A). Since bundle sheath strands can be separated easily (Covshoff et al., 2013) leaves of
143 C_4 species provide a simple system to study transcription factor binding in specific cells (Figure
144 2B). After bundle sheath isolation from *S. bicolor, S. italica* and *Z. mays* a total of 129,137 DHS
145 were identified (Figure 2B; Table S4) containing 452,263 DGF (Figure 2B; Table S4; FDR<0.01).
146 Of the 452,263 DGF identified in bundle sheath strands, 170,114 were statistically enriched in the
147 bundle sheath samples compared with whole leaves (Figure 2B; Table S4). The number of these
148 statistically enriched DGF in bundle sheath strands of C_4 species was large and ranged from
149 15,880 to 85,256 in maize and *S. italica* respectively (Figure S3). Genome-wide, the number of
150 broad regulatory regions defined by DHS in the bundle sheath that overlapped with those present
151 in whole leaves ranged from 71 to 84% in *S. italica* and *S. bicolor* respectively (Table S5).
152 However, only 8-23% of the narrower DGF found in the bundle sheath were also identified in whole
153 leaves (Table S6). Taken together, these findings indicate that specific cell types of leaves share
154 considerable similarity in the broad regions of DNA that are accessible to transcription factors, but
155 that the short sequences actually bound by transcription factors vary dramatically.

156 To provide evidence that DGF predicted after analysis of separated bundle sheath strands are
157 of functional importance, they were compared with previously validated *cis*-elements. In C_4
158 species, there are few such examples, but in the maize *RbcS* gene, which is preferentially
159 expressed in bundle sheath cells, an I-box (GATAAG) is essential for light-mediated activation

160 (Giuliano et al., 1988) and a HOMO motif (CCTTTTTTCCTT) is important in driving bundle sheath
161 expression (Xu et al., 2001) (Figure 2C). Both elements were detected in our pipeline. Interestingly,
162 the HOMO motif was only bound in the bundle sheath strands (Figure 2C), and whilst the I-box
163 was detected in both bundle sheath strands and whole leaves, the position of the DGF covering it
164 was slightly shifted between the two samples (Figure 2C). Thus, orthogonal evidence for
165 transcription factor binding in maize supports a functional role for DGF identified by DNaseI-SEQ in
166 this study.

167 To investigate the relationship between cell specific gene expression and the position of DHS
168 and DGF, the DNase-I data were compared with RNA-seq datasets from mesophyll and bundle
169 sheath cells of C_4 leaves (Chang et al., 2012; Emms et al., 2016; John et al., 2014). At least three
170 mechanisms associated with cell specific gene expression operating around individual genes were
171 identified, and can be exemplified using three co-linear genes found on chromosome seven of *S.*
172 *bicolor*. First, in the NADP-malate dehydrogenase (*MDH)* gene, which is highly expressed in
173 mesophyll cells and encodes a protein of the core C_4 cycle (Figure S4) a broad DHS site was
174 present in whole leaves, but not in bundle sheath strands (Figure 2D). Whilst presence of this site
175 indicates accessibility of DNA to transcription factors that could activate expression in mesophyll
176 cells, global analysis of all genes strongly and preferentially expressed in bundle sheath strands
177 indicates that presence/absence of a DHS in the bundle sheath compared with the whole leaf is
178 not sufficient to generate cell specificity (Figure S5, S6). Second, in the next contiguous gene that
179 encodes an additional isoform of MDH that is also preferentially expressed in mesophyll cells
180 (Figure S4) a DHS was found in both whole leaf and bundle sheath strands but DGF occupancy
181 within this region differed between cell types (Figure 2D). Thus, despite similarity in DNA
182 accessibility, the binding of particular transcription factors was different between cell types.
183 However, once again, genome-wide analysis indicated that alterations to individual DGF were not
184 sufficient to explain cell specific gene expression. For example, fewer than 30% of all enriched
185 DGF in the bundle sheath were associated with differentially expressed genes (Table S7). Lastly,
186 in the third gene in this region, which encodes a NAC domain transcription factor preferentially
187 expressed in bundle sheath strands, differentially enriched DGF were associated both with regions
188 of the gene that have similar DHS in each cell type, but also a region lacking a DHS in whole

189 leaves compared with bundle sheath strands (Figure 2D). These three classes of alteration to
190 transcription factor accessibility and binding were detectable in genes encoding core components
191 of the C_4 cycle (Figure 2E, Figure S7) implying that a complex mosaic of altered transcription factor
192 binding mediates the cell specific expression found in the C_4 leaf.

193 Overall, we conclude that differences in transcription factor binding between cells is associated
194 with both DNA accessibility defined by broad DHS, as well as fine-scale alterations to transcription
195 factor binding defined by DGF. In addition, although bundle sheath strands possessed a distinct
196 regulatory landscape compared with the whole leaf, we were unable to identify examples of C_4
197 genes in which individual transcription factor binding sites differed between bundle sheath and
198 whole leaf samples. This finding implies that cell specific gene expression in C_4 leaves is mediated
199 by a complex mixture of combinatorial effects mediated by alterations to gene accessibility as
200 defined by DHS, but also changes to binding of multiple transcription factors to each C_4 gene.

201

202 **Transcription factor families associated with cell specific expression**

203 The cistrome, or set of transcription factor binding sites found in a genome, has been
204 determined for *A. thaliana* and to date, consists of 872 experimentally verified motifs linked to 529
205 transcription factors (O'Malley et al., 2016). Of these 872 motifs from *A. thaliana* 525 could be
206 identified in the *Z. mays*, *S. bicolor, S. italica* and *B. distachyon* datasets (Figure 3A). However,
207 within individual species fewer motifs were detected and so *de novo* prediction was used to identify
208 sequences over-represented in DGF compared with those across the whole genome. This resulted
209 in an additional 524 novel motifs being annotated (Figure 3A). Inspection of these motifs predicted
210 *de novo* demonstrated clear strand bias in DNase-I cuts (Figure 3B) as would expected from *bone*
211 *fide* transcription factor binding. By combining known and *de novo* motifs, the percentage of DGF
212 that could be annotated in each species increased to more than 41% (Figure 3C). The relatively
213 high number of motifs defined by transcription factor binding sites predicted *de novo* is presumably
214 due to the significant evolutionary time since grasses diverged from *A. thaliana*.

215 To define the most common motifs actually bound by transcription factors in mature leaves
216 undertaking C_3 and C_4 photosynthesis the frequency of individual motifs was determined and
217 ranked from most to least common in each species. The relative ranking of motifs in the four

218 grasses was similar (Figure 3D). Visualisation of transcription factor families associated with these
219 DGF in word clouds showed that the most prevalent motifs are associated with the AP2-EREBP
220 and C2H2 transcription factor families (Figure 3D). These findings indicate that across these four
221 grasses the most commonly bound transcription factor motifs are highly conserved. There was
222 much less conservation between transcription factor binding sites in photosynthetic leaves of these
223 monocotyledons compared with the dicotyledon *A. thaliana* (Figure 3D). This finding combined with
224 the large number of motifs from *A. thaliana* not detected in the grasses (Figure 3A) argue for
225 significant divergence in the cistromes of monocotyledons and dicotyledons.

226 To investigate whether particular classes of transcription factor binding motifs are associated
227 with specific genomic features, the proportion of each motif found in promoter elements, 5' UTRs,
228 coding regions, introns and 3' UTR sequences was defined (Figure S8). In most cases, the
229 distribution of individual motifs was similar in all genomic features, however it was noticeable that a
230 set of motifs was particularly common in coding sequence (Figure S8). Clustering analysis
231 indicated that a set of 96 transcription factor motifs were strongly associated with coding
232 sequences in all four grass species (Figure S9B, S10). The clear strand-bias indicates strong
233 protein-DNA interaction centred on these motifs within coding sequences (Figure S9C). Sequences
234 that carry out a dual role in both coding for amino acids and in transcription factor binding have
235 been termed duons. Thus, in grasses it appears that duons are recognised by a specific set of
236 transcription factors.

237 To identify regulatory factors associated with gene expression in the C_4 bundle sheath,
238 transcription factor motifs located in DGF enriched in either the bundle sheath or in whole leaf
239 samples of *S. bicolor* were identified (Figure 3E). There was little difference in the ranking of the
240 most prevalent commonly used motifs between these cell types (Figure 3E&F). For example, the
241 AP2-EREBP and C2H2 families were dominant in both bundle sheath and whole leaf samples,
242 indicating that cell-specificity is not associated with large-scale changes in the relative importance
243 of transcription factor binding. However, in terms of prevalence, a small number of transcription
244 factor binding motifs were ranked in the top 50% in whole leaves but the bottom 50% in bundle
245 sheath strands (Figure 3F). This finding implies that quantitative modifications to the use of

246 particular transcription factor families are associated with the spatial patterning of gene expression
247 that is a hallmark of C_4 photosynthesis.

248 Further analysis revealed that in all three C_4 species, motifs recognised by C2C2GATA, bZIP,
249 bHLH, BZR and TCP transcription factors were enriched in whole leaf samples, whereas those
250 bound by ARID transcription factors were enriched in the bundle sheath (Figure 3G and Table S9).
251 Moreover, analysis of the cell-specific transcript accumulation of members of the C2C2-GATA
252 family, revealed one orthologue which was consistently mesophyll enriched in all three C_4 species
253 (GRMZM2G379005, Seita.1G358400, Sobic.004G337500; Figure 3H). Thus, these data implicate
254 these transcription factor families in controlling cell-specific gene expression in C_4 leaves, and
255 indicate that in some cases, separate C_4 lineages appear to be using orthologous transcription
256 factors to drive cell specific expression.

257

258 **Transcription factor binding sites that are conserved but mobile**

259 As *B. distachyon, S. bicolor, Z. mays* and *S. italica* are thought to have diverged from a
260 common ancestor around 60 million years ago (The International Brachypodium Initiative, 2010)
261 they provide an opportunity to examine the extent to which the *cis*-regulatory code has diverged
262 since that point. Furthermore, whilst the last common ancestor of *Z. mays* and *S. bicolor* was
263 thought to use C_4 photosynthesis, *S. italica* belongs to a separate C_4 lineage (Zhang et al., 2012a).
264 Thus, comparative analysis of these species should provide insight into the extent to which the *cis*-
265 regulatory architecture is conserved in the grasses, and how it has been modified during the
266 evolution of C_4 photosynthesis.

267 In pairwise comparisons of the four species, DGF fell into three categories: those for which
268 homologous sequences were both present and bound by a transcription factor (conserved and
269 occupied), those for which homologous sequences were present but were only bound by a
270 transcription factor in one species (conserved but not occupied) and those for which no sequence
271 homology could be found (not conserved) (Figure 4A). Only a small percentage of DGF were both
272 conserved in sequence and bound by transcription factors (Figure 4B, Table S8). DGF that were
273 conserved but unoccupied were the next most abundant group (Figure 4B) but the majority of DGF

274 were not conserved (Figure 4B, Table S8). These data indicate substantial turnover in the *cis*-code
275 associated with the transcription factor binding repertoire of monocotyledons.

276 Consistent with the rapid turnover of DGF documented genome-wide (Figure 4B), the majority
277 of C_4 genes did not share DGF (Table S10 and S11). However, three genes associated with the
278 core C_4 and the Calvin-Benson-Bassham cycle that are strongly expressed in either bundle sheath
279 or mesophyll cells contained the same *cis*-elements bound by a transcription factor in all three C_4
280 species. For example, in the 2-oxoglutarate/malate transporter (*OMT1*) gene, four sites defined by
281 transcription factor binding were detected in all three C_4 species (Figure 4C). However, the position
282 of these sites within the gene varied in each species. In the transketolase (*TKL*) gene that is
283 preferentially expressed in bundle sheath cells, three conserved motifs defined by transcription
284 factor binding were detected in all C_4 species, but they were also all found in the C_3 species *B.*
285 *distachyon* (Figure 4D). Thus, in some cases patterning of C_4 gene expression appears linked to
286 pre-existing regulatory architecture operating in the ancestral C_3 state, but in cases where the *cis*-
287 regulatory code associated with C_4 gene expression is strongly conserved the position of these
288 transcription factor binding sites within any gene is variable.

289

290 **Hyper-conserved *cis*-regulators found in coding sequences of C_4 genes**

291 To investigate the extent to which transcription factor binding sites associated with C_4 genes
292 within a C_4 lineage are conserved, genes encoding the core C_4 cycle were compared in *S. bicolor*
293 and *Z. mays* (Figure 5A). 28 genes associated with the C_4 and Calvin-Benson-Bassham Cycles
294 contained a total of 531 DGF. Although many of these transcription factor footprints were
295 conserved in sequence within orthologous genes, only twenty were both conserved and bound by
296 a transcription factor (Figure 5A). These data therefore indicate that although many *cis*-elements
297 found in orthologous genes of the C_4 cycle are conserved in sequence, a small proportion were
298 bound by a transcription factor at the time of sampling.

299 Genome-wide, the number of DGF that were conserved in sequence and bound by a
300 transcription factor decayed in a non-linear manner with phylogenetic distance (Figure 5B). For
301 example, *Z. mays* and *S. bicolor* shared 9,446 DGF that were both conserved and occupied. *S.*
302 *italica* shared only 1,194 DGF with *Z. mays* and *S. bicolor* (Figure 5B). Finally, comparison of these

303 C_4 grasses with C_3 *B. distachyon* yielded 192 DGF that have been conserved over >60Myr of
304 evolution. 95 of these highly conserved DGF were present in whole leaf samples of the C_3 species,
305 but in the C_4 species were restricted to the bundle sheath (Figure 5B). This set of 192 ancient and
306 highly conserved DGF were located predominantly in 5' UTRs and coding sequence and strikingly,
307 in bundle sheath strands, over fifty percent of these hyper-conserved DGF were in coding
308 sequence (Figure 5B).

309 One such hyper-conserved DGF is found in the *NdhM* gene that encodes a subunit of the
310 NADH complex that preferentially assembles in bundle sheath cells of C_4 plants (Figure 5C) but it
311 is not known how this evolved. In the ancestral C_3 state a hyper-conserved DGF is found in whole
312 leaves of *B. distachyon* (Figure 5D). However, in all three C_4 species rather than this DGF being
313 detected in whole leaf material, it is detected in the bundle sheath. It is also noticeable that this
314 motif has proliferated within the gene in the C_4 species compared with C_3 *B. distachyon*, and in
315 maize and sorghum is also found in the 5' UTR as well as coding sequence. Furthermore, in whole
316 leaf samples of these C_4 species, transcription factor binding is shifted upstream or downstream
317 (Figure 5D). We therefore propose that preferential expression of *NdhM* in the bundle sheath is
318 built upon a *cis*-regulator present in the C_3 state that activates expression in all photosynthetic cells
319 of the leaf. During the evolution of C_4 photosynthesis, whilst accessibility of this ancient and highly
320 conserved *cis*-element is maintained in the bundle sheath to allow expression of *NdhM,* in
321 mesophyll cells an additional transcription factor(s) binds flanking sequence that blocks access to
322 this pre-existing architecture. These findings are consistent with hyper-conserved DGF located in
323 coding sequence playing an important role in the cell specific gene expression required in leaves of
324 C_4 grasses.

325 As genome-wide analysis indicated that a specific group of DGF was associated with coding
326 sequence (Figure S8-S10) we investigated whether motifs associated with the 192 hyper-
327 conserved DGF found in all four grasses were over-represented in this set. Remarkably, of the 96
328 families of transcription factors strongly associated with binding motifs in coding sequence (Figure
329 S10), 47 and 55 were hyper-conserved in the whole leaf and bundle sheath respectively and the
330 ERF family was particularly common (Figure S11, S12). Overall, these data indicate that in these
331 grasses specific families of transcription factors are particularly important in binding coding

sequences, and that the duons bound by these transcription factors are highly conserved across deep evolutionary time.

Discussion

Genome-wide transcription factor binding in grasses

The data presented here provide insight into genome-wide binding of transcription factors in photosynthetic tissue, but also maize and sorghum which represent two of the world's most productive crops. This transcription factor binding landscape shows both similarities and differences with other eukaryotic systems. For example, in contrast with *A. thaliana* in which AT-rich DNA is preferentially bound, the grasses showed preferential binding of transcription factors to GC-rich DNA. Preference for GC-rich DNA has also been observed in humans (Wang et al., 2012) and so the differences in binding likely reflect the relative proportion of nucleotides in each genome. In all these eukaryotes, individual genes are bound by a complex mosaic of transcription factors distributed across major genic feature including promoter regions, UTRs and coding sequence. However, in grasses this standard architecture exemplified by yeast, animals and *A. thaliana* appears to be have been modified such that a much higher proportion of transcription factor footprints are located in exonic and coding regions. For example, in human cells ~3% of transcription factor binding sites are exonic (Stergachis et al., 2013). In contrast, in grass leaves studied here up to 36% and 25% of transcription factor binding sites were located in exonic and coding sequence respectively. This finding is supported by the following observations. First, within individual genes the distribution of transcription factor binding sites peaked after the predicted transcriptional start site. Second, in grasses, strong and reproducible expression of transgenes is routinely achieved by fusing 5' exon and intron sequence to the promoter of interest (Cornejo et al., 1993; Jeon et al., 2000; Maas et al., 1991). Third, although the functional importance of transcription factor binding to coding sequences has been debated in animals (Xing and He, 2015), in grasses these motifs are bound by specific families of transcription factors, and so it is not the case that all transcription factors contribute to this non-random distribution. Moreover, in plants functional analysis has now indicated that duons can control the patterning of gene expression (Reyna-Llorens et al., 2016). Although it is unclear why transcription factor binding in grasses should be particularly prevalent in 5' UTR and coding sequences, these findings combined with the available literature argue for duons and the cognate transcription factors that bind them being of pervasive importance in grass genomes.

364

365 **The transcription factor landscape underpinning gene expression in specific cell types**

366 Given the central importance of cellular compartmentation to C_4 photosynthesis, there have
367 been significant efforts to identify *cis*-elements that restrict gene expression to either mesophyll or
368 bundle sheath cells of C_4 leaves (Hibberd and Covshoff, 2010; Sheen, 1999; Wang et al., 2014).
369 Along with many other systems, initial analysis focussed on regulatory elements located in
370 promoters of C_4 genes (Sheen, 1999) but, it has become increasingly apparent that the patterning
371 of gene expression between cells in the C_4 leaf can be mediated by elements in various parts of a
372 gene. This includes untranslated regions (Kajala et al., 2011; Patel et al., 2004; Viret et al., 1994;
373 Williams et al., 2016; Xu et al., 2001) and coding sequences (Brown et al., 2011; Reyna-Llorens et
374 al., 2016). The genome-wide data reported here provides an unbiased insight into where
375 transcription factors bind C_4 genes, and along with the rest of the genome, indicate that binding is
376 most dense in the 5' UTRs and coding exons.

377 Mechanistically, this DNaseI dataset also indicates that cell specific gene expression in C_4
378 leaves is not strongly correlated with changes to large-scale accessibility of DNA as defined by
379 DHS. This strongly implies that modifications to chromatin density within any one gene do not
380 impact on its expression between cell types. Rather, as only 8-24% of transcription factor binding
381 sites detected in the bundle sheath were also found in whole leaves, the data strongly implicate
382 complex modifications to patterns of transcription factor binding in controlling gene expression
383 between cell types. These findings are consistent with analogous analysis in roots where genes
384 with clear spatial patterns of expression are bound by multiple transcription factors (Sparks et al.,
385 2016) and highly combinatorial interactions between multiple activators and repressors tune the
386 output (de Lucas et al., 2016). However, it is also the case that particular classes of transcription
387 factors including the C2C2GATA, bZIP, bHLH and ARID families are implicated in patterning of
388 gene expression because they were preferentially detected as binding their cognate *cis*-elements
389 in either bundle sheath strands or whole leaves. Our findings therefore strongly imply that the
390 spatial patterning of gene expression in leaves is mediated by a quantitative switch in the
391 abundance of a group of transcription factors.

392 More generally, the finding that so few transcription factor binding sites were shared between
393 different cell types in leaves of *S. bicolor, Z. mays* and *S. italica* argues strongly for the need to
394 isolate these cells when attempting to understand the control of gene expression. Although
395 separating bundle sheath strands from C_4 leaves is relatively trivial (Covshoff et al., 2013; Furbank
396 et al., 1985; Leegood, 1985) this is not the case for C_3 leaves. Approaches in which nuclei from
397 specific cell-types are labelled with an exogenous tag (Deal and Henikoff, 2011) should now allow
398 their transcription factor landscapes to be defined. In the future, the application of DNase I-SEQ to
399 specific cell types from both C_3 and C_4 leaves should provide insight into how the extent to which
400 gene regulatory networks have been re-wired during the evolution of the complex C_4 trait.
401

402 **Characteristics of the transcription factor repertoire facilitating evolution of the C_4 pathway**

403 Comparison of transcription factor binding in the C_3 grass *B. distachyon* with three C_4 species
404 provides insight into mechanisms associated with the evolution of C_4 photosynthesis. One striking
405 finding was that in all four species, irrespective of whether they used C_3 or C_4 photosynthesis, the
406 most abundant DNA motifs bound by transcription factors were similar. Thus, motifs recognised by
407 the AP2EREBP, C2C2 and C2C2DOF classes of transcription factor were most commonly bound
408 across each genome. This indicates that during the evolution of C_4 photosynthesis, there has been
409 relatively little alteration to the most abundant classes of transcription factors that bind DNA.

410 The repeated evolution of the C_4 pathway has frequently been associated with convergent
411 evolution (Sage, 2004; Sage et al., 2012). However, parallel alterations to amino acid and
412 nucleotide sequence that allow altered kinetics of the C_4 enzymes (Christin et al., 2014, 2007) and
413 patterning of C_4 gene expression (Brown et al., 2011) respectively have also been reported. The
414 genome-wide analysis of transcription factor binding now indicates that parallel evolution of
415 transcription factors has contributed to the repeated appearance of C_4 photosynthesis. This is best
416 exemplified by the fact that in the three C_4 species that are derived from two independent C_4
417 lineages, motifs bound by the ARID and C2C2GATA classes of transcription factor were enriched
418 in bundle sheath and whole leaves respectively. In the case of the C2C2GATA family, transcripts
419 derived from one specific orthologue were more abundant in mesophyll cells of all C_4 species.
420 Thus, within separate lineages of C_4 plant, the same classes of transcription factors have been

421 recruited into functioning preferentially in one cell type, and in the case of the C2C2GATA family
422 this is associated with orthologous genes being preferentially expressed in mesophyll cells.

423 When orthologous genes were compared between genomes the majority of transcription factor
424 binding sites were not conserved. Furthermore, of the DGF that were conserved, we found that
425 their position within orthologous genes varied. This indicates that C_4 photosynthesis in grasses is
426 tolerating both a rapid turnover of the *cis*-code, and that when motifs are conserved in sequence,
427 their position and number within a gene can vary. It therefore appears that the cell-specific
428 accumulation patterns of C_4 proteins can be maintained despite considerable modifications to the
429 cistrome of C_4 leaves. This finding is analogous to the situation in yeast where the output of
430 genetic circuits can be maintained despite rapid turnover of regulatory mechanisms underpinning
431 them (Tsong et al., 2006). It was also the case that some conserved motifs bound by transcription
432 factors in the C_4 species were present in *B. distachyon*, which uses the ancestral C_3 pathway.
433 Previous work has shown that *cis*-elements used in C_4 photosynthesis can be found in orthologous
434 genes from C_3 species (Reyna-Llorens et al., 2016; Williams et al., 2016). However, these previous
435 studies identified *cis*-elements that were conserved in both sequence and position. As it is now
436 clear that such conserved sites are mobile within a gene, it seems likely that many more examples
437 of ancient *cis*-elements important in C_4 photosynthesis will be found in C_3 plants.

438 Although we were able to detect a small number of transcription factor binding sites that were
439 conserved and occupied in all four species that were sampled, these ancient hyper-conserved
440 motifs appear to have played a role in the evolution of C_4 photosynthesis. Interestingly, a large
441 proportion of these motifs bound by transcription factors are found in coding sequence, and this
442 bias was particularly noticeable in bundle sheath cells. Due to the amino acid code, the rate of
443 mutation of coding sequence compared with the genome is restricted. If such regions have a
444 longer half-life than transcription factor binding sites in other regions of the genome, then they may
445 represent an excellent source of raw material for the repeated evolution of complex traits (Martin
446 and Orgogozo, 2013). It remains to be determined why this characteristic is particularly noticeable
447 in bundle sheath cells of C_4 leaves.

448 In summary, the data presented here provides a transcription factor binding atlas for leaves of
449 grasses using either C_3 or C_4 photosynthesis. Surprisingly, many sequences bound by transcription

factors are found within genes rather than promoter regions. Indeed, particular transcription factor families preferentially bind coding sequence and the motifs that they bind are highly conserved in the grasses. Moreover, the canonical patterning of gene expression in C_4 leaves is underpinned by complex combinatorial modifications to transcription factor binding. Lastly, consistent with the deep evolutionary time associated with the divergence of the monocotyledons and dicotyledons, the cistrome of grasses is highly divergent from that of the model plant *Arabidopsis thaliana*.

456 **Figure Legends:**

457 **Figure 1: Transcription factor binding atlas for whole leaf samples of four grasses.** (A)
458 Schematic of phylogenetic relationship between species analysed. The two independent origins of
459 C_4 photosynthesis are highlighted with black and white circles. (B) Summary of sampling and the
460 total number of DNase I-hypersensitive sites (DHS) and Digital Genomic Footprints (DGF)
461 identified across all four species. (C) TreeView diagrams illustrating cut density around individual
462 digital genomic footprint (DGF). Each row represents an individual DGF, cuts are coloured
463 according to whether they align to the positive (red) or negative (blue) strand and indicate
464 increased cutting in a 50 bp window on either side of the DGF. The total number of DGF per
465 sample is shown at the bottom. (D) Representation of DNase I-SEQ data from *S. bicolor*, depicting
466 gene (grey), DHS (light blue), DGF (orange) and DNase-I cut density (dark blue) at five scales:
467 genome wide, with chromosome number and position indicated (top), chromosomal (second level),
468 kb genomic region (third level), individual *PPC* gene (fourth level) and individual transcription factor
469 binding sites (fifth level). Between each level the expanded area is illustrated. (E) Pie-chart
470 representing the distribution of DGF among genomic features. Promoters are defined as 3000
471 base pairs (bp) upstream the transcriptional start site while downstream and intergenic features
472 represent regions 1000 and >1000bp downstream of the transcription termination site respectively.
473 (F) Density of DGF per kb in each genomic feature.

474

475 **Figure 2: Characterisation of the DNA binding landscape in the C_4 Bundle Sheath.** (A)
476 Schematic showing that footprints associated with low abundance cells such as the Bundle Sheath
477 (BS) may not be detected from whole leaf (WL) samples. (B) Bundle sheath isolation for DNase I-
478 SEQ experiments, with phylogeny (left) and workflow (right). (C) DGF identified in the maize
479 *ZmRBCS3* gene coincide with I- and HOMO-boxes known to regulate gene expression. The gene
480 model is annotated with whole leaf (blue) and BS (orange) DGF, and the I- and HOMO-boxes are
481 indicated below. (D) Co-linear genes from *S. bicolor* depicting three classes in alterations to DNA
482 accessibility and transcription factor binding to genes that are differentially expressed between
483 whole leaf (blue) and bundle sheath (orange). The C_4 *MDH* contains a DHS and consequently
484 DGF only in the whole leaf, the non-C_4 MDH contains the same DHS but shows variation in DGF

485 between the cell-types, and the NAC transcription factor contains DGF derived from both regions
486 that share DHS, but also one that lack a DHS in the whole leaf sample. (E) Representation of the
487 core C_4 pathway showing differentially accessible DHS, DGF and cell-specific DGF in whole leaf
488 (blue) and bundle sheath (orange) samples of *S. bicolor*. CA; Carbonic Anhydrase, PEPC;
489 Phospho*enol*pyruvate carboxylase, PPDK; Pyruvate,orthophosphate dikinase, MDH; Malate
490 dehydrogenase, NADP-ME; NADP- dependent malic enzyme, RBCS1A; Ribulose bisphosphate
491 carboxylase small subunit 1A, OAA; Oxaloacetate, Mal; Malate, PEP; Phospho*enol*pyruvate, Pyr;
492 Pyruvate, Asp; Aspartate.
493
494 **Figure 3: Distinct cistromes in monocotyledons and dicotyledons.** (A) Number of previously
495 reported motifs as well as those defined *de novo* in the grasses. (B) Density plots depicting
496 average DNase-I activity on positive (red) and negative (blue) strands centred around a *de novo*
497 motif. (C) Bar chart depicting percentage of DGF annotated with known or *de novo* motifs. (D)
498 Comparison of TF motif prevalence in Whole Leaf (WL) samples from *S. italica*, *Z. mays*, *B.*
499 *distachyon* and *A. thaliana* compared with *S. bicolor*. Word clouds depict frequency of motifs
500 associated with transcription factor families, with larger names more abundant. Scatter plots
501 compare frequency of transcription factor motifs within DGF, ranked from low (most abundant) to
502 high (least abundant). Correlation between samples is indicated as Kendell's Tau coefficient (τ).
503 (E) Comparison of transcription factor motif prevalence in BS enriched and whole leaf enriched
504 DGF from *S. bicolor*. Word clouds depict frequency of motifs associated with transcription factor
505 families. (F) Frequency plots of transcription factor motifs in whole leaf or BS samples ranked from
506 low to high. Motifs that ranked in the top 50% most prevalent in one cell type and the bottom 50%
507 in the other are depicted in red. (G) Diagram summarising motifs associated with specific
508 transcription factor families that are over-represented in BS or whole leaves from *S. italica, S.*
509 *bicolor and Z. mays*. The most common transcription factor families are represented. (H)
510 Scatterplots comparing mean transcript per million (TPM) values in bundle sheath and mesophyll
511 cells (data from Chang et al., 2012; Emms et al., 2016; John et al., 2014) for members of the
512 C2C2-GATA family *in S. bicolor, Z. mays* and *S. italica.* Orthologous genes that are consistently
513 enriched in mesophyll cells are highlighted in red.

514 **Figure 4: *Cis*-elements show high rates of turnover and mobility in grasses.** (A) Scenarios of
515 DGF conservation between species. Reads derived from DNase-I cuts are depicted by grey, DGF
516 that are both conserved and occupied between species by red, and DGF that are conserved but
517 unoccupied by blue shading. (B) Bar-plot representing pairwise comparisons of DGF occupancy.
518 (C&D) Schematic depicting the position of four transcription factor motifs that are consistently
519 associated with oxaloacetate transporter (*OMT1*) in *S. bicolor, Z. mays* and *S. italica* (C) and three
520 transcription factor motifs that are consistently associated with the bundle sheath enriched gene
521 *TKL* in *S. bicolor, Z. mays*, *S. italica* and C_3 *B. distachyon* (D). The relative position of conserved
522 motifs between orthologous genes is depicted by solid lines (blue, orange, green) and varies
523 between species.
524
525 **Figure 5: Hyper-conserved *cis*-elements in grasses recruited into C_4 photosynthesis.** (A)
526 Conservation of *cis*-regulation in C_4 and Calvin Benson Bassham cycle genes following the
527 divergence of *Z. mays* and *S. bicolor.* The number of carbon atoms (red dots) and metabolite flow
528 (red dashed line) between mesophyll (grey) and bundle sheath (orange) cells are illustrated along
529 with the degree of conservation of DGF associated with BS strands. (B) Conservation of DGF
530 occupancy in grasses across evolutionary time. Results are depicted for whole leaf (WL - blue) and
531 bundle sheath (BS - orange) DGF. Pie-charts display the distribution of conserved and occupied
532 DGF for whole leaf and BS strands. Promoters are defined as 3000bp upstream the transcriptional
533 start site while downstream and intergenic features represent 1000 and >1000bp downstream of
534 the transcription termination site respectively. (C) Evolution of *cis*-regulation in *NdhM* - the BS is
535 enriched in the *Ndh* complex that takes part in cyclic electron flow (CEF). *NdhM* transcript
536 abundance is higher in BS than M cells of C_4 species (data from Chang et al., 2012; Emms et al.,
537 2016; John et al., 2014). (D) DGF in orthologous *Ndh* sequences (grey) and conserved and
538 occupied (red). A single DGF is conserved in all four monocot species. In the ancestral C_3 state
539 this footprint is present in whole leaf samples, but in the derived C_4 state it is occupied in the BS.
540 An additional footprint is present upstream or downstream in whole leaf tissues which may prevent
541 binding in mesophyll cells.
542

543 **Figure S1:** DNase-I digestion of nuclei for sequencing. Representative images of digested
544 samples separated on a 2% (w/v) agarose gels by electrophoresis. (A) *S. bicolor* WL (B) *S. bicolor*
545 BS (C) *Z. mays* WL (D) *Z. mays* BS (E) *B. distachyon* WL (F) *S. italica* WL (G) *S, italica* BS. Each
546 gel represents a separate biological replicate, and the units of DNase-I used are illustrated above.
547 Samples selected for sequencing are indicated in red.
548
549 **Figure S2:** Density plots depicting the distribution of DGF -4000 to +4000 base pairs from the
550 transcriptional start site (TSS) of *S. bicolor, Z. mays, S. italica* and *B. distachyon* whole leaves. In
551 each case, the distribution shows greater transcription factor binding after the transcriptional start
552 site.
553
554 **Figure S3:** Bar chart depicting the number of DGF statistically enriched in bundle sheath cells of *S.*
555 *bicolor, Z. mays* and *S. italica*.
556
557 **Figure S4:** Transcript abundance expressed as transcripts per million reads (TPM) of three co-
558 linear genes on chromosome seven of sorghum. C_4 *MDH* (Sobic.007G166300.1), non C_4 *MDH*
559 (non C_4, Sobic.007G166200.1), and an uncharacterised *NAC* domain protein
560 (Sobic.007G166100.1) in BS or M cells.
561
562 **Figure S5:** Gene expression in mesophyll and bundle sheath cells associated DHS and DGF in *S.*
563 *bicolor*. (A) Cell preferential gene expression profiles of highly abundant M and BS genes
564 expressed as transcripts per million reads (TPM). (B) Schematic representing DHS, DGF and DE
565 DGF present in WL (blue) and BS (orange) of *S. bicolor*.
566
567 **Figure S6:** Differential accessibility of broad regulatory regions in *S. bicolor* is not sufficient for cell
568 preferential gene expression. Percentage of differentially detected DHS among BS and M specific
569 genes (n=50) in *S. bicolor* compared against randomly generated gene samples.
570

571 **Figure S7:** Representation of the C_4 pathway showing differentially accessible DHS, DGF and cell
572 specific DGF between whole leaf (blue) and bundle sheath (orange) samples in *S. italica* (A) and *Z.*
573 *mays* (B). CA; Carbonic Anhydrase, PEPC; Phospho*enol*pyruvate carboxylase, PPDK; Pyruvate,
574 orthophosphate dikinase, MDH; Malate dehydrogenase, NADP-ME; NADP-dependent malic
575 enzyme, RBCS1A; Ribulose bisphosphate carboxylase small subnut1A, OAA; Oxaloacetate, Mal;
576 Malate, PEP; Phospho*enol*pyruvate, Pyr; Pyruvate, Asp; Aspartate.
577
578 **Figure S8:** Proportion of motifs from whole leaf DGF in each genomic feature of *S. bicolor*, *Z.*
579 *mays, S. italica* and *B. distachyon*. The majority of motifs are distributed across all genomic
580 features, and so the proportion associated with any one feature is relatively low. However, a set of
581 motifs are enriched in coding sequences.
582
583 **Figure S9:** A group of 96 motifs are preferentially associated with coding sequences in grasses.
584 (A) Proportion of all annotated motifs in coding sequence for *S. bicolor* compared with *Z. mays, S.*
585 *italica* and *B. distachyon*. (B) Heatmap showing the association of motifs with each genomic
586 feature. The horizontal bar at the top represents five clusters obtained by k-means. Hierarchical
587 clustering was used to group genomic features in *S. bicolor* (Sb)*, Z. mays* (Zm)*, S. italica* (Si) and
588 *B. distachyon* (Bd). (C) Representative motifs associated with coding sequences in *S. bicolor* (top).
589 TreeView diagrams illustrating cut density around representative motifs in coding sequences
590 (middle). Each row represents an individual DGF, cuts are coloured according to strand alignment.
591 The number of motif hits in coding sequence are listed in the left. Density plots depicting average
592 DNase I activity on positive (red) and negative (blue) strands centred around motifs are shown at
593 the bottom.
594
595 **Figure S10:** Distribution within genomic features of 96 motifs associated with DGF in coding
596 sequences from whole leaves of *S. bicolor, Z. mays, S. italica* and *B. distachyon*.
597

598 **Figure S11:** Distribution within genomic features of 47 motifs associated with DGF in coding
599 sequences and found within hyper-conserved DGF (Figure 5) from whole leaves of *S. bicolor, Z.*
600 *mays, S. italica* and *B. distachyon*.
601
602 **Figure S12:** Distribution within genomic features of 55 motifs associated with DGF in coding
603 sequences and found within hyper-conserved DGF (Figure 5) from bundle sheath strands of *S.*
604 *bicolor, Z. mays, S. italica* and *B. distachyon*.
605

606 **Table S1: Summary of DNAse-SEQ Quality Metrics**. Values were calculated according to (Landt
607 et al., 2012) and include the number of reads mapped following filtering (NMAP), PCR bottleneck
608 Coefficient (PCB), Normalized Strand Cross-correlation Coefficient (NSC), Relative Strand Cross-
609 correlation Coefficient (RSC) the optimal number of peaks calculated by IDR method (PEAKS),
610 and the Signal Portion Of Tags (SPOT) for WL and BS samples from *B. distachyon*, *S. italica*, *S.*
611 *bicolor* and *Z. mays*.
612
613 **Table S2: Summary Statistics for Genomic Features Identified in Whole Leaf Samples.**
614 Including information about the number of DHS and DGF identified per sample, and the number of
615 genes that could be annotated with at least one genomic feature for *B. distachyon*, *S. italica*, *S.*
616 *bicolor* and *Z. mays*.
617
618 **Table S3: Base-pair percentages in DGFs and the genome of *S. bicolor*, *Z. mays*, *S. italica***
619 **and *B. distachyon.***
620
621 **Table S4: Summary Statistics for Genomic Features Identified in Bundle Sheath Samples.**
622 Including information about the number of DHS and DGF identified per sample, and the number of
623 genes that could be annotated with at least one genomic feature for *B. distachyon*, *S. italica*, *S.*
624 *bicolor* and *Z. mays*.
625
626 **Table S5: Summary Statistics of Overlap between DHS in Whole Leaf and Bundle Sheath**
627 **Samples.**
628
629 **Table S6: Summary Statistics of Overlap between DGF in Whole Leaf and Bundle Sheath**
630 **Samples.**
631
632 **Table S7: Summary Statistics for Differential Digital Genomic Footprint Calling.** Including the
633 total number of differential DGF (DE DGF) and the number of DE DGF in DE genes for *S. italica*,
634 *S. bicolor* and *Z. mays*.

635

636 **Table S8: Statistics for Cross Mapping of genomic features between *S. bicolor*, *S. italica*, *Z.***
637 ***mays* and *B. distachyon*.**

638

639 **Table S9: TF family motifs enriched (FDR<0.05) in differential footprints from *S.***
640 ***bicolor, Z. mays* and *S. italica* WL and BS samples.**

641

642 **Table S10: Identifiers of orthologous C_4 and CBB cycle related genes from *S. bicolor*, *S.***
643 ***italica*, *Z. mays* and *B. distachyon*.**

644

645 **Table S11: C_4 and CCB genes associated with the same known or *de novo* transcription**
646 **factor binding motifs in *Z. mays*, *S. bicolor*, *S. italica* and *B. distachyon.***

647 **Methods**

648 **Growth conditions and isolation of nuclei**

649 *S. bicolor*, *S. italica* and *Z. mays* were grown under controlled conditions at the University of
650 Cambridge in a chamber set to 12h/12h light/dark; 28°C light/20°C dark; 400µmol m^{-2} s^{-1} photon
651 flux density, 60% humidity. For germination, *S. bicolor* and *Z. mays* seeds were imbibed in dH_2O
652 for 48h, *S. italica* seeds were incubated on wet filter paper at 30°C overnight in the dark. *Z. mays*,
653 *S. bicolor* and *S. italica* were grown on 3:1 (v/v) M3 compost to medium vermiculite mixture, with a
654 thin covering of soil. Seedlings were hand-watered. For *B. distachyon* plants were grown under
655 controlled conditions at the Sainsbury Laboratory Cambridge University, first under short day
656 conditions 14h/10h, light/dark for 2 weeks and then shifted to long day 20h/4h, light/dark, for 1
657 week and harvested at ZT20. Temperature was set at 20°C, humidity 65% and light intensity
658 350µmol m^{-2} s^{-1}.

659 To isolate nuclei from *S. bicolor*, *Z. mays* and *S. italica* mature third and fourth leaves with a
660 fully developed ligule were harvested 4-6 h into the light cycle on the 18th day after germination.
661 Bundle sheath cells were mechanically isolated (Covshoff et al., 2013). At least 3 g of tissue was
662 used for each extraction. Nuclei were isolated using a sucrose gradient adapted from (Gendrel et
663 al., 2005) and the amount of nuclei in each preparation was quantified using a haemocytometer.
664 For *B. distachyon* plants were flash frozen and material pulverised in a coffee grinder. 3g of plant
665 material was added to 45 ml NIB buffer (10mM Tris-HCl, 0.2M sucrose, 0.01% (v/v) Triton X-100,
666 pH 5.3 containing protease inhibitors (SIGMA)) and incubated at 4°C on a rotating wheel for 5 min,
667 afterwards debris was removed by sieving through 2 layers of Miracloth (millipore) into pre-cooled
668 flasks. Nuclei were spun down 4,000rpm, 4°C for 20 min. Plastids were lysed by adding Triton to
669 a final concentration of 0.3% (v/v) and incubated for 15 min on ice. Nuclei were pelleted
670 by centrifugation at 5000 rpm at 4°C for 15 min. Pellets were washed 3 times with chilled NIB
671 buffer.

672

673 **DNAse-I digestion, sequencing and library preparation**

674 To obtain sufficient DNA each biological replicate consisted of leaves from tens of individuals
675 and to conform to standards set by the Human Genome project at least two biological replicates

676 were sequenced for each sample. 2 x 10^8 of freshly extracted nuclei were re-suspended at 4°C in
677 digestion buffer (15 mM Tris-HCl, 90 mM NaCl, 60 mM KCl, 6 mM $CaCl_2$, 0.5 mM spermidine, 1
678 mM EDTA and 0.5 mM EGTA, pH 8.0). DNAse-I (Fermentas) at 7.5 U was added to each tube and
679 incubated at 37 °C for 3 min. Digestion was arrested with addition of 1:1 volume of stop buffer (50
680 mM Tris-HCl, 100 mM NaCl, 0.1% (w/v) SDS, 100 mM EDTA, pH 8.0, 1 mM Spermidine, 0.3mM
681 Spermine, RNase A 40 µg/ml) and incubated at 55°C for 15 min. 50 U of Proteinase K was added
682 and samples incubated at 55 °C for 1 h. DNA was isolated with 25:24:1 Phenol:Chloroform:Isoamyl
683 Alcohol (Ambion) followed by ethanol precipitation. Samples were then size-selected using
684 agarose gel electrophoresis. The extracted DNA samples were quantified fluorometrically with a
685 Qubit 3.0 Fluorometer (Life technologies), and a total of 10 ng of digested DNA (200 pg l^{-1}) was
686 used for library construction.

687 Initial sample quality control of pre-fragmented DNA was assessed using a Tapestation DNA
688 1000 High sensitivity Screen tape (Agilent, Cheadle UK). Sequencing ready libraries were
689 prepared using the Hyper Prep DNA Library preparation kit (Kapa Biosystems, London UK)
690 according to the manufacturer's instructions and indexed for pooling using NextFlex DNA barcoded
691 adapters (Bioo Scientific, Austin TX US). Libraries were quantified using a Tapestation DNA 1000
692 Screen tape and by qPCR using an NGS Library Quantification Kit (KAPA Biosystems) on an
693 AriaMx qPCR system (Agilent) and then normalised, pooled, diluted and denatured for sequencing
694 on the NextSeq 500 (Illumina, Chesterford UK). The main library was spiked at 10% with the PhiX
695 control library (Illumina). Sequencing was performed using Illumina NextSeq in the Departments of
696 Biochemistry and Pathology at the University of Cambridge, UK, with 2x75 cycles of sequencing.

697

698 **Data processing**

699 Genome sequences were downloaded from Phytozome (v10) (Goodstein et al., 2012). The
700 following genome assemblies were used: Bdistachyon_283_assembly_v2.0; Sbicolor_255_v2.0;
701 Sitalica_164_v2; Zmays_284_AGPv3. Reads were mapped to genomes using bowtie2 (Langmead
702 and Salzberg, 2012) with the following parameters:

703

704 --local –D 15 –R 2 –N 0 –L 20 –I S,1,0.75.

705

706 Aligned reads were then processed using samtools (Li et al., 2009) to remove those with a MAPQ
707 score <42. DHS sites were identified using a procedure adapted from the ENCODE 3 pipeline
708 (https://sites.google.com/site/anshulkundaje/projects/idr) (Marinov et al., 2014). Briefly DHS were
709 called using MACS2 (Feng et al., 2012) with the following parameters to offset read locations in
710 order to position DHS cut site in the middle of peak regions:

711

712 -p 1e-1 –nomodel –extsize 150 –shift -75 –llocal 50000

713

714 The final set of peak calls were determined using the irreproducible discovery rate (IDR (Li et al.,
715 2011)) and calculated using the script batch_consistency_analysis.R
716 (https://github.com/modENCODE-DCC/Galaxy/blob/master/modENCODE_DCC_tools/idr/batch-
717 consistency-analysis.r).

718

719 **Quality metrics and identification of Digital Genomic Footprints (DGF)**

720 SPOT score (number of a subsample of mapped reads (5M) in DHS/Total number of
721 subsampled, mapped reads (5M) (John et al., 2011)) was calculated using BEDTools (Quinlan and
722 Hall, 2010) to determine the number of mapped reads possessing at least 1bp overlap with a DHS
723 site. NSC and RSC scores were calculated using SPP (Kharchenko et al., 2008) and PCR
724 bottleneck coefficient (PCB) was calculated using BEDTools and the following bash code:

```
725 bedtools bamtobed –bedpe –I ${FILT_BAM_FILE_n} | awk 'BEGIN{OFS="\t"}{print
726 $1,$2,$4,$6,$9,$10}' | grep –v 'ChrM\ChrC'| sort | uniq –c | awk 'BEGIN{mt=0;m0=0;m1=0;m2=0}
727 ($1==1){m1=m1+1} ($1==2){m2=m2+1} {m0=m0+1} {mt=mt+$1} END{printf
728 "%d\t%d\t%d\t%d\t%f\t%f\t%f\n",mt,m0,m1,m2,m0/mt,m1/m0,m1/m2}' > ${PBC_FILE_QC}`
```

729

730 Digital Genomic Footprints (DGF) were identified using the Wellington algorithm (Piper et al., 2013)
731 in the pyDNase software package (http://pythonhosted.org/pyDNase/) with the following
732 parameters:

733 -fdr 0.05 [regions] [reads] [output directory]

where [reads] represents a BED file of DHS locations within which footprints were called and [reads] a filtered BAM file of sequenced reads.

Differential DGF were identified using Wellington bootstrap algorithm (Piper et al., 2015) from pyDNase package with the following parameters:

```
-fdr 0.05 [treatment_BAM] [control_BAM] [regions] [treatment_output] [control_output]
```

Where [treatment_BAM] is a filtered BAM file containing sequenced reads from the sample of interest, [control_BAM] is a filtered BAM file containing mapped sequenced reads against sample for comparison; [regions] is a BED file containing DHS locations within which footprints are called. All DE DGFs with a threshold of score equal and higher than 10 were considered as differentially abundant DGFs.

Data visualisation

DHS and DGF sequences were loaded into and visualized in the Integrative Genomics Viewer (Thorvaldsdóttir et al., 2013) and figures produced in Inkscape, bar plots were generated with R package ggplot2 (Wickham, 2009), scatterplots using R function plot() and figures depicting conservation of DGF or motifs between orthologous sequences were generated using genoplotR (Guy et al., 2010). Word clouds were created with the wordcloud R package (Fellows, 2012).

TreeView images were produced in two stages. The script ‘dnase_to_javatreeview.py’ from pyDNAse was run with the following parameters to generate the input file:

```
[regions_BED] [reads_BAM] [OUTPUT]
```

Where [regions_BED] is a bed file containing locations of all DGF sites, [reads_BAM] is the BAM file containing all aligned reads, and [OUTPUT] specifies the output csv file name. To visualize files Java TreeView (Saldanha, 2004) was run with the following command:

```
java -Xmx4G -jar TreeView.jar
```

Changing the file format settings to All Files, the csv file from pyDNase was loaded into TreeView, from the dropdown menu entered Settings->Pixel Setting and checked all the Fill boxes, Contrast Value 1 and colours Red and Blue, the output was saved as .svg file.

Average cut density plots were generated using the script 'dnase_average_profile.py' from pyDNase (Piper et al., 2013, 2015) with the following parameters:

```
–w 100 –b [regions_BED] [reads_BAM] [OUTPUT]
```

Where [regions_BED] is a bed file containing locations of all DGF sites, [reads_BAM] is the BAM file containing all aligned reads, and [OUTPUT] specifies the output file name.

Genomic features were annotated and distribution calculated using the Bioconductor package ChIPpeakAnno (Zhu, 2013; Zhu et al., 2010a) interfaced with a custom R script. The required gff3 files (Goodstein et al., 2012) (Sitalica_164_v2.1.gene_exons.gff3; Sbicolor_255_v2.1.gene_exons.gff3; Zmays_284_6a.gene.exons.gff3; Bdistachyon_283_v2.1.gene_exons.gff3) downloaded from Phytozome.

In order to convert motif files into MEME format for motif scanning a multi-step procedure was necessary. Background frequency files are required when generating motifs (Thijs et al., 2001); to produce background files FASTA sequences for the regions of interest (DGF) were extracted using BEDTools suite (Quinlan and Hall, 2010) with the following command:

```
bedtools getfasta -fi [FASTA_genome] -bed [regions]-fo [FASTA_regions]
```

Background frequency files were tailored for each species for motif searching, using scripts from the meme suite (Bailey et al., 2009).

```
fasta-get-markov [FASTA_all] [background_file_MEME]
```

Motif files in FASTA format were converted to STAMP format using the online tool (http://www.benoslab.pitt.edu/stamp/) (Mahony and Benos, 2007), then RSTAT was used to convert STAMP format into TRANSFAC format (http://rsat01.biologie.ens.fr/rsa-tools/convert-matrix_form.cgi) (Medina-Rivera et al., 2015). A bug in the transfac2meme script requires that all bp frequencies are represented as floating point numbers containing two decimal places. In order to convert the TRANSFAC file to a suitable format the following code was used:

```
sed 's/0 /0.00/g' [transfac file] | sed 's/1 /1.00/g' | sed 's/2 /2.00/g' | sed 's/3 /3.00/g' | sed 's/4 /4.00/g' | sed 's/5 /5.00/g' | sed 's/6 /6.00/g' | sed 's/7 /7.00/g' | sed 's/8 /8.00/g' | sed 's/9 /9.00/g' | sed 's/0$/0.00/g' | sed 's/1$/1.00/g' | sed 's/2$/2.00/g' | sed 's/3$/3.00/g' | sed 's/4$/4.00/g' | sed 's/5$/5.00/g' | sed 's/6$/6.00/g' | sed 's/7$/7.00/g' | sed 's/8$/8.00/g' | sed 's/9$/9.00/g' | sed 's/\P0.00 /\P0/g' > [transfac_fixed]
```

MEME motif files were created from TRANSFAC files using scripts from the MEME suite (Bailey et al., 2009) with the following command:

```
transfac2meme -bg [background_file] [transfac_fixed] > [MEME_FILE]
```

where [background_file] is the background base pair distribution file and [MEME_FILE] is the motif file output.

de novo motif prediction, motif scanning and enrichment testing

de novo motif prediction was performed using findMotifsGenome.pl script from the HOMER suite (Heinz et al., 2010) using digital genomic footprints (DGF) as input together with the reference genome sequence for each species with the following command:

```
findMotifsGenome.pl [INPUT_DGFs.bed] [REF_GENOME.fasta] [OUTFILE].motifs -size 200 -cpg
```

A set of 872 transcription factor binding motifs (O'Malley et al., 2016) in meme format was downloaded from

821 http://neomorph.salk.edu/dev/pages/shhuang/dap_web/pages/browse_table_aj.php

822 Motif scanning was performed using FIMO (Grant et al., 2011) with default parameters:

823

824 --bgfile [background_file] --o [OUPUT_FILE] [MOTIF_FILE] [FASTA_REGIONS]

825

826 where [background_file] is the background base pair distribution file, [OUTPUT_FILE] is the output
827 file name, [MOTIF_FILE] is the file containing input motif(s) in MEME format and
828 [FASTA_REGIONS] is a FASTA file containing all DGF sequences motifs are scanned against.

829 To determine overrepresentation of TF family motifs in samples hypergeometric tests were
830 performed using R with the following parameters:

831 over<-phyper(hitInSample-1,hitInPop,failInPop,sampleSize,lower.tail=F)

832 where:

833 Population: Unique genes with an annotation in whole leaf and bundles sheath samples.

834 sampleSize: Number of unique genes with an annotation in whole leaf samples.

835 HitInPop: Total number of unique genes annotated with given transcription factor in tissue sample.

836 HitInSample: Number of unique genes sharing an annotation in WL and BS samples (overlap).

837 failInPop: Number of unique genes with annotation only in WL samples.

838 p-values were adjusted for the false discovery rate using the procedure of Benjamini & Hochberg
839 (Benjamini and Hochberg, 1995).

840

841 The distribution of each motif across different genomic features was obtained for each of the 525
842 known annotated motifs by dividing the number of hits in a particular feature by the total number of
843 hits in the genome. K-means clustering was then employed to group motifs by genomic feature in
844 *Z. mays, S. italica, S. bicolor and B. distachyon*.

845

846 **Whole genome alignments and pairwise cross mapping of genomic features**

847 To cross map genomic features between species, mapping files were generated according to
848 (http://genomewiki.ucsc.edu/index.php/Whole_genome_alignment_howto) using tools from the

849 UCSC Genome Browser, including trfBig, faToNib, faSize, lavToPsl, faSplit, axtChain, chainNet
850 (Kent et al., 2002) and LASTZ (Harris, 2007).
851 Genomic features where then mapped between genomes using bnMapper (Denas et al., 2015)
852 and the following parameters:
853
854 -fBED4 –threshold 0.7 –o [outfile] [infile] [Chain file]
855
856 where [infile] is a BED file of DGF locations in the species of origin, [Chain file] is a chain file
857 providing mapping coordinates between the species of origin and comparison.
858
859 **Data**
860 Detailed step by step methods are available for DNase I digestion are on protocols.io
861 (dx.doi.org/10.17504/protocols.io.hdfb23n), Raw sequencing data and processed files are
862 deposited in Gene Expression Omnibus (GSE97369).
863
864 **Contributions:** SJB and I-RL grew and harvested nuclei from *S. bicolor*, *S. italica* and *Z. mays*. KJ
865 provided the nuclei from *B. distachyon*. SJB and I-RL performed DNase I digestion and data
866 analysis. SJB, I-RL and JMH wrote the manuscript and prepared the figures.
867
868 **Acknowledgements:** KJ was supported by a Gatsby Career Development Fellowship, IRL was
869 supported by CONCyT and BBSRC grant BB/L014130, whilst SJB was supported by the *3to4*
870 grant from the EU and BB/I002243 from the BBSRC.

871 **References**

872 Bailey, T.L., Boden, M., Buske, F.A., Frith, M., Grant, C.E., Clementi, L., Ren, J., Li, W.W., and
873 Noble, W.S. (2009). MEME Suite: tools for motif discovery and searching. Nucleic Acids Res. *37*,
874 W202–W208.
875 Bauwe, H., Hagemann, M., and Fernie, A.R. (2010). Photorespiration: players, partners and origin.
876 Trends Plant Sci. *15*, 330–336.
877 Benjamini, Y., and Hochberg, Y. (1995). Controlling the False Discovery Rate: A Practical and
878 Powerful Approach to Multiple Testing. J. R. Stat. Soc. Ser. B *57*, 289–300.
879 Bowes, G., Ogren, W.L., and Hageman, R.H. (1971). Phosphoglycolate production catalyzed by
880 ribulose diphosphate carboxylase. Biochem. Biophys. Res. Commun. *45*, 716–722.
881 Brown, N.J., Newell, C.A., Stanley, S., Chen, J.E., Perrin, A.J., Kajala, K., and Hibberd, J.M.
882 (2011). Independent and Parallel Recruitment of Preexisting Mechanisms Underlying C_4
883 Photosynthesis. Science *331*, 1436–1439.
884 Chang, Y.M., Liu, W.Y., Shih, A.C., Shen, M.N., Lu, C.H., Lu, M.Y., Yang, H.W., Wang, T.Y., Chen,
885 S.C., Chen, S.M., et al. (2012). Characterizing regulatory and functional differentiation between
886 maize mesophyll and bundle sheath cells by transcriptomic analysis. Plant Physiol *160*, 165–177.
887 Christin, P.-A., Salamin, N., Savolainen, V., Duvall, M.R., and Besnard, G. (2014). C_4
888 Photosynthesis Evolved in Grasses via Parallel Adaptive Genetic Changes. Curr. Biol. *17*, 1241–
889 1247.
890 Christin, P.A., Salamin, N., Savolainen, V., Duvall, M.R., and Besnard, G. (2007). C_4
891 photosynthesis evolved in grasses via parallel adaptive genetic changes. Curr. Biol. *17*, 1241–
892 1247.
893 Cornejo, M.-J., Luth, D., Blankenship, K.M., Anderson, O.D., and Blechl, A.E. (1993). Activity of a
894 maize ubiquitin promoter in transgenic rice. Plant Mol. Biol. *23*, 567–581.
895 Covshoff, S., Furbank, R.T., Leegood, R.C., and Hibberd, J.M. (2013). Leaf rolling allows
896 quantification of mRNA abundance in mesophyll cells of sorghum. J Exp Bot *64*, 807–813.
897 Deal, R.B., and Henikoff, S. (2011). The INTACT method for cell type-specific gene expression and
898 chromatin profiling in Arabidopsis thaliana. Nat. Protoc. *6*, 56–68.
899 Denas, O., Sandstrom, R., Cheng, Y., Beal, K., Herrero, J., Hardison, R.C., and Taylor, J. (2015).

900 Genome-wide comparative analysis reveals human-mouse regulatory landscape and evolution.
901 BMC Genomics *16*, 87.
902 Emms, D.M., Covshoff, S., Hibberd, J.M., and Kelly, S. (2016). Independent and Parallel Evolution
903 of New Genes by Gene Duplication in Two Origins of C_4 Photosynthesis Provides New Insight into
904 the Mechanism of Phloem Loading in C_4 Species. Mol. Biol. Evol. *33*, 1796–1806.
905 Fellows, I. (2012). wordcloud: Word clouds. R Packag. Version *2*, 109.
906 Feng, J., Liu, T., Qin, B., Zhang, Y., and Liu, X.S. (2012). Identifying ChIP-seq enrichment using
907 MACS. Nat. Protoc. *7*, 1728–1740.
908 Furbank, R.T. (2011). Evolution of the C_4 photosynthetic mechanism: are there really three C_4 acid
909 decarboxylation types? J. Exp. Bot. *62*, 3103–3108.
910 Furbank, R.T., Stitt, M., and Foyer, C.H. (1985). Intercellular compartmentation of sucrose
911 synthesis in leaves of Zea mays L. Planta *164*, 172–178.
912 Gendrel, A.-V., Lippman, Z., Martienssen, R., and Colot, V. (2005). Profiling histone modification
913 patterns in plants using genomic tiling microarrays. Nat Meth *2*, 213–218.
914 Goodstein, D.M., Shu, S., Howson, R., Neupane, R., Hayes, R.D., Fazo, J., Mitros, T., Dirks, W.,
915 Hellsten, U., Putnam, N., et al. (2012). Phytozome: a comparative platform for green plant
916 genomics. Nucleic Acids Res. *40*, D1178-86.
917 Gowik, U., Burscheidt, J., Akyildiz, M., Schlue, U., Koczor, M., Streubel, M., and Westhoff, P.
918 (2004). cis-Regulatory elements for mesophyll-specific gene expression in the C_4 plant *Flaveria*
919 *trinervia*, the promoter of the C_4 phospho*enol*pyruvate carboxylase gene. Plant Cell *16*, 1077–
920 1090.
921 Grant, C.E., Bailey, T.L., and Noble, W.S. (2011). FIMO: scanning for occurrences of a given motif.
922 Bioinforma. *27*, 1017–1018.
923 Guy, L., Roat Kultima, J., and Andersson, S.G.E. (2010). genoPlotR: comparative gene and
924 genome visualization in R. Bioinformatics *26*, 2334–2335.
925 Harris, R.S. (2007). Improved pairwise alignment of genomic DNA. The Pennsylvania State
926 University.
927 Hatch, M.D. (1987). C_4 photosynthesis: a unique blend of modified biochemistry, anatomy and
928 ultrastructure. Biochim. Biophys. Acta *895*, 81–106.

929 Heinz, S., Benner, C., Spann, N., Bertolino, E., Lin, Y.C., and Laslo, P. (2010). Simple
930 combinations of lineage-determining transcription factors prime cis-regulatory elements required
931 for macrophage and B cell identities. Mol. Cell. *38*.
932 Hesselberth, J.R., Chen, X., Zhang, Z., Sabo, P.J., Sandstrom, R., Reynolds, A.P., Thurman, R.E.,
933 Neph, S., Kuehn, M.S., Noble, W.S., et al. (2009). Global mapping of protein-DNA interactions in
934 vivo by digital genomic footprinting. Nat. Methods *6*, 283–289.
935 Hibberd, J.M., and Covshoff, S. (2010). The regulation of gene expression required for C_4
936 photosynthesis. Annu Rev Plant Biol *61*, 181–207.
937 Jeon, J.-S., Lee, S., Jung, K.-H., Jun, S.-H., Kim, C., and An, G. (2000). Tissue-Preferential
938 Expression of a Rice α-Tubulin Gene, OsTubA1, Mediated by the First Intron. Plant Physiol. *123*,
939 1005–1014.
940 John, C.R., Smith-Unna, R.D., Woodfield, H., Covshoff, S., and Hibberd, J.M. (2014). Evolutionary
941 Convergence of Cell-Specific Gene Expression in Independent Lineages of C_4 Grasses. Plant
942 Physiol. *165*, 62–75.
943 John, S., Sabo, P.J., Thurman, R.E., Sung, M.-H., Biddie, S.C., Johnson, T.A., Hager, G.L., and
944 Stamatoyannopoulos, J.A. (2011). Chromatin accessibility pre-determines glucocorticoid receptor
945 binding patterns. Nat Genet *43*, 264–268.
946 Jordan, D.B., and Ogren, W.L. (1984). The CO_2/O_2 specificity of Ribulose 1,5-Bisphosphate
947 Carboxylase Oxygenase - dependence on Ribulose bisphosphate concentration, pH and
948 temperature. Planta *161*, 308–313.
949 Kajala, K., Williams, B.P., Brown, N.J., Taylor, L.E., and Hibberd, J.M. (2011). Multiple Arabidopsis
950 genes primed for direct recruitment into C_4 photosynthesis. Plant J. *69*, 47–56.
951 Kent, W.J., Sugnet, C.W., Furey, T.S., Roskin, K.M., Pringle, T.H., Zahler, A.M., and Haussler,
952 and D. (2002). The Human Genome Browser at UCSC. Genome Res. *12*, 996–1006.
953 Kharchenko, P. V, Tolstorukov, M.Y., and Park, P.J. (2008). Design and analysis of ChIP-seq
954 experiments for DNA-binding proteins. Nat Biotech *26*, 1351–1359.
955 Kromdijk, J., Głowacka, K., Leonelli, L., Gabilly, S.T., Iwai, M., Niyogi, K.K., and Long, S.P. (2016).
956 Improving photosynthesis and crop productivity by accelerating recovery from photoprotection.
957 Science *354*, 857–861.

958 Landt, S.G., Marinov, G.K., Kundaje, A., Kheradpour, P., Pauli, F., and Batzoglou, S. (2012). ChIP-
959 seq guidelines and practices of the ENCODE and modENCODE consortia. Genome Res *22*.
960 Langmead, B., and Salzberg, S.L. (2012). Fast gapped-read alignment with Bowtie 2. Nat Meth *9*,
961 357–359.
962 Leakey, A.D.B., Bishop, K.A., and Ainsworth, E.A. (2012). A multi-biome gap in understanding of
963 crop and ecosystem responses to elevated CO_2. Curr. Opin. Plant Biol. *15*, 228–236.
964 Leegood, R.C. (1985). The intercellular compartmentation of metabolites in leaves of *Zea mays* L.
965 Planta *164*, 163–171.
966 Lefebvre, S., Lawson, T., Fryer, M., Zakhleniuk, O. V, Lloyd, J.C., and Raines, C.A. (2005).
967 Increased Sedoheptulose-1,7-Bisphosphatase Activity in Transgenic Tobacco Plants Stimulates
968 Photosynthesis and Growth from an Early Stage in Development. Plant Physiol. *138*, 451–460.
969 Li, H., Handsaker, B., Wysoker, A., Fennell, T., Ruan, J., Homer, N., Marth, G., Abecasis, G.,
970 Durbin, R., and Subgroup, 1000 Genome Project Data Processing (2009). The Sequence
971 Alignment/Map format and SAMtools. Bioinformatics *25*, 2078–2079.
972 Li, Q., Brown, J.B., Huang, H., and Bickel, P.J. (2011). Measuring reproducibility of high-throughput
973 experiments. Ann. Appl. Stat. *5*, 1752–1779.
974 Long, S.P., Marshall-Colon, A., and Zhu, X.-G. (2015). Meeting the Global Food Demand of the
975 Future by Engineering Crop Photosynthesis and Yield Potential. Cell *161*, 56–66.
976 Maas, C., Laufs, J., Grant, S., Korfhage, C., and Werr, W. (1991). The combination of a novel
977 stimulatory element in the first exon of the maize Shrunken-1 gene with the following intron 1
978 enhances reporter gene expression up to 1000-fold. Plant Mol. Biol. *16*, 199–207.
979 Mahony, S., and Benos, P. V (2007). STAMP: a web tool for exploring DNA-binding motif
980 similarities. Nucleic Acids Res. *35*, W253–W258.
981 Marinov, G.K., Kundaje, A., Park, P.J., and Wold, B.J. (2014). Large-Scale Quality Analysis of
982 Published ChIP-seq Data. G3 *4*, 209–223.
983 Martin, A., and Orgogozo, V. (2013). The Loci of repeated evolution: a catalog of genetic hotspots
984 of phenotypic variation. Evolution *67*, 1235–1250.
985 Matsuoka, M., and Numazawa, T. (1991). *Cis*-acting elements in the pyruvate, orthophosphate
986 dikinase gene from maize. Mol. Gen. Genet. *228*, 143–152.

987 Medina-Rivera, A., Defrance, M., Sand, O., Herrmann, C., Castro-Mondragon, J.A., Delerce, J.,
988 Jaeger, S., Blanchet, C., Vincens, P., Caron, C., et al. (2015). RSAT 2015: Regulatory Sequence
989 Analysis Tools. Nucleic Acids Res. 43: W50-W56.
990 Miyagawa, Y., Tamoi, M., and Shigeoka, S. (2001). Overexpression of a cyanobacterial fructose-
991 1,6-/sedoheptulose-1,7-bisphosphatase in tobacco enhances photosynthesis and growth. Nat.
992 Biotechnol. *19*, 965–969.
993 Neph, S., Vierstra, J., Stergachis, A.B., Reynolds, A.P., Haugen, E., Vernot, B., Thurman, R.E.,
994 John, S., Sandstrom, R., Johnson, A.K., et al. (2012). An expansive human regulatory lexicon
995 encoded in transcription factor footprints. Nature *489*, 83–90.
996 O'Malley, R.C., Huang, S.C., Song, L., Lewsey, M.G., Bartlett, A., Nery, J.R., Galli, M., Gallavotti,
997 A., and Ecker, J.R. (2016). Cistrome and Epicistrome Features Shape the Regulatory DNA
998 Landscape. Cell *165*, 1280–1292.
999 Ort, D.R., Merchant, S.S., Alric, J., Barkan, A., Blankenship, R.E., Bock, R., Croce, R., Hanson,
1000 M.R., Hibberd, J.M., Long, S.P., et al. (2015). Redesigning photosynthesis to sustainably meet
1001 global food and bioenergy demand. Proc. Natl. Acad. Sci. *112*, 8529–8536.
1002 Patel, M., Corey, A.C., Yin, L.P., Ali, S.J., Taylor, W.C., and Berry, J.O. (2004). Untranslated
1003 regions from C-4 amaranth AhRbcS1 mRNAs confer translational enhancement and preferential
1004 bundle sheath cell expression in transgenic C_4 *Flaveria bidentis*. Plant Physiol. *136*, 3550–3561.
1005 Piper, J., Elze, M.C., Cauchy, P., Cockerill, P.N., Bonifer, C., and Ott, S. (2013). Wellington: a
1006 novel method for the accurate identification of digital genomic footprints from DNase-seq data.
1007 Nucleic Acids Res. *41*, e201-e201.
1008 Piper, J., Assi, S.A., Cauchy, P., Ladroue, C., Cockerill, P.N., Bonifer, C., and Ott, S. (2015).
1009 Wellington-bootstrap: differential DNase-seq footprinting identifies cell-type determining
1010 transcription factors. BMC Genomics *16*, 1000.
1011 Quinlan, A.R., and Hall, I.M. (2010). BEDTools: a flexible suite of utilities for comparing genomic
1012 features. Bioinforma. *26*, 841–842.
1013 Reyna-Llorens, I., Burgess, S.J., Williams, B.P., Stanley, S., Boursnell, C., and Hibberd, J.M.
1014 (2016). Ancient coding sequences underpin the spatial patterning of gene expression in C_4 leaves.
1015 bioRxiv doi: https://doi.org/10.1101/085795.

1016 Sage, R. (2004). The evolution of C_4 photosynthesis. New Phytol. *161*, 341–370.

1017 Sage, R.F., and Zhu, X.-G. (2011). Exploiting the engine of C_4 photosynthesis. J. Exp. Bot. *62*,
1018 2989–3000.

1019 Sage, R.F., Christin, P.-A., and Edwards, E.J. (2011). The C_4 plant lineages of planet Earth. J.
1020 Exp. Bot. *62*, 3171–3181.

1021 Sage, R.F., Sage, T.L., and Kocacinar, F. (2012). Photorespiration and the evolution of C_4
1022 photosynthesis. Annu. Rev. Plant Biol. *63*, 19–47.

1023 Saldanha, A.J. (2004). Java Treeview--extensible visualization of microarray data. Bioinformatics.
1024 *20*.

1025 Sharwood, R.E., Ghannoum, O., Kapralov, M. V, Gunn, L.H., and Whitney, S.M. (2016).
1026 Temperature responses of Rubisco from Paniceae grasses provide opportunities for improving C_3
1027 photosynthesis. Nat. Plants *2*, 16186.

1028 Sheen, J. (1999). C_4 gene expression. Ann. Rev Plant Physiol. Plant Mol Biol *50*, 187–217.

1029 Stergachis, A.B., Haugen, E., Shafer, A., Fu, W., Vernot, B., Reynolds, A., Raubitschek, A.,
1030 Ziegler, S., LeProust, E.M., Akey, J.M., et al. (2013). Exonic transcription factor binding directs
1031 codon choice and affects protein evolution. Science *342*, 1367–1372.

1032 The International Brachypodium Initiative (2010). Genome sequencing and analysis of the model
1033 grass Brachypodium distachyon. Nature *463*, 763–768.

1034 Thijs, G., Lescot, M., Marchal, K., Rombauts, S., De Moor, B., Rouzé, P., and Moreau, Y. (2001). A
1035 higher-order background model improves the detection of promoter regulatory elements by Gibbs
1036 sampling. Bioinformatics *17*, 1113–1122.

1037 Thorvaldsdóttir, H., Robinson, J.T., and Mesirov, J.P. (2013). Integrative Genomics Viewer (IGV):
1038 high-performance genomics data visualization and exploration. Briefings Bioinforma. *14*, 178–192.

1039 Thurman, R.E., Rynes, E., Humbert, R., Vierstra, J., Maurano, M.T., Haugen, E., Sheffield, N.C.,
1040 Stergachis, A.B., Wang, H., Vernot, B., et al. (2012). The accessible chromatin landscape of the
1041 human genome. Nature *489*, 75–82.

1042 Tolbert, N.E. (1971). Microbodies - peroxisomes and glyoxysomes. Annu. Rev. Plant Physiol. *22*,
1043 45–74.

1044 Tsong, A.E., Tuch, B.B., Li, H., and Johnson, A.D. (2006). Evolution of alternative transcriptional

1045 circuits with identical logic. Nature *443*, 415–420.

1046 Viret, J.F., Mabrouk, Y., and Bogorad, L. (1994). Transcriptional photoregulation of cell-type
1047 preferred expression of maize rbcS-m3: 3' and 5' sequences are involved. Proc. Natl. Acad. Sci.
1048 *91*, 8577–8581.

1049 Wang, J., Zhuang, J., Iyer, S., Lin, X., Whitfield, T.W., Greven, M.C., Pierce, B.G., Dong, X.,
1050 Kundaje, A., Cheng, Y., et al. (2012). Sequence features and chromatin structure around the
1051 genomic regions bound by 119 human transcription factors. Genome Res. *22*, 1798–1812.

1052 Wang, L., Czedik-Eysenberg, A., Mertz, R.A., Si, Y., Tohge, T., Nunes-Nesi, A., Arrivault, S.,
1053 Dedow, L.K., Bryant, D.W., Zhou, W., et al. (2014). Comparative analyses of C_4 and C_3
1054 photosynthesis in developing leaves of maize and rice. Nat Biotech *32*, 1158–1165.

1055 Wickham, H. (2009). ggplot2: elegant graphics for data analysis (Springer New York).

1056 Williams, B.P., Burgess, S.J., Reyna-Llorens, I., Knerova, J., Aubry, S., Stanley, S., and Hibberd,
1057 J.M. (2016). An untranslated cis-element regulates the accumulation of multiple C_4 enzymes in
1058 Gynandropsis gynandra mesophyll cells. Plant Cell *28*, 454–465.

1059 Xing, K., and He, X. (2015). Reassessing the "Duon" Hypothesis of Protein Evolution. Mol. Biol.
1060 Evol. *32*, 1056–1062.

1061 Xu, T., Purcell, M., Zucchi, P., Helentjaris, T., and Bogorad, L. (2001). TRM1, a YY1-like
1062 suppressor of rbcS-m3 expression in maize mesophyll cells. Proc. Natl. Acad. Sci. U. S. A. *98*,
1063 2295–2300.

1064 Zentner, G.E., and Henikoff, S. (2014). High-resolution digital profiling of the epigenome. Nat Rev
1065 Genet *15*, 814–827.

1066 Zhang, G., Liu, X., Quan, Z., Cheng, S., Xu, X., Pan, S., Xie, M., Zeng, P., Yue, Z., Wang, W., et
1067 al. (2012a). Genome sequence of foxtail millet (*Setaria italica*) provides insights into grass
1068 evolution and biofuel potential. Nat Biotech *30*, 549–554.

1069 Zhang, W., Wu, Y., Schnable, J.C., Zeng, Z., Freeling, M., Crawford, G.E., and Jiang, J. (2012b).
1070 High-resolution mapping of open chromatin in the rice genome. Genome Res. *22*, 151–162.

1071 Zhu, L.J. (2013). Integrative Analysis of ChIP-Chip and ChIP-Seq Dataset BT - Tiling Arrays:
1072 Methods and Protocols. T.-L. Lee, and A.C. Shui Luk, eds. (Totowa, NJ: Humana Press), pp. 105–
1073 124.

1074 Zhu, L.J., Gazin, C., Lawson, N.D., Pagès, H., Lin, S.M., Lapointe, D.S., and Green, M.R. (2010a).
1075 ChIPpeakAnno: a Bioconductor package to annotate ChIP-seq and ChIP-chip data. BMC
1076 Bioinformatics *11*, 237.
1077 Zhu, X., Long, S., and Ort, D. (2010b). Improving Photosynthetic Efficiency for Greater Yield. Annu.
1078 Rev. Plant Biol. *61*, 235–261.

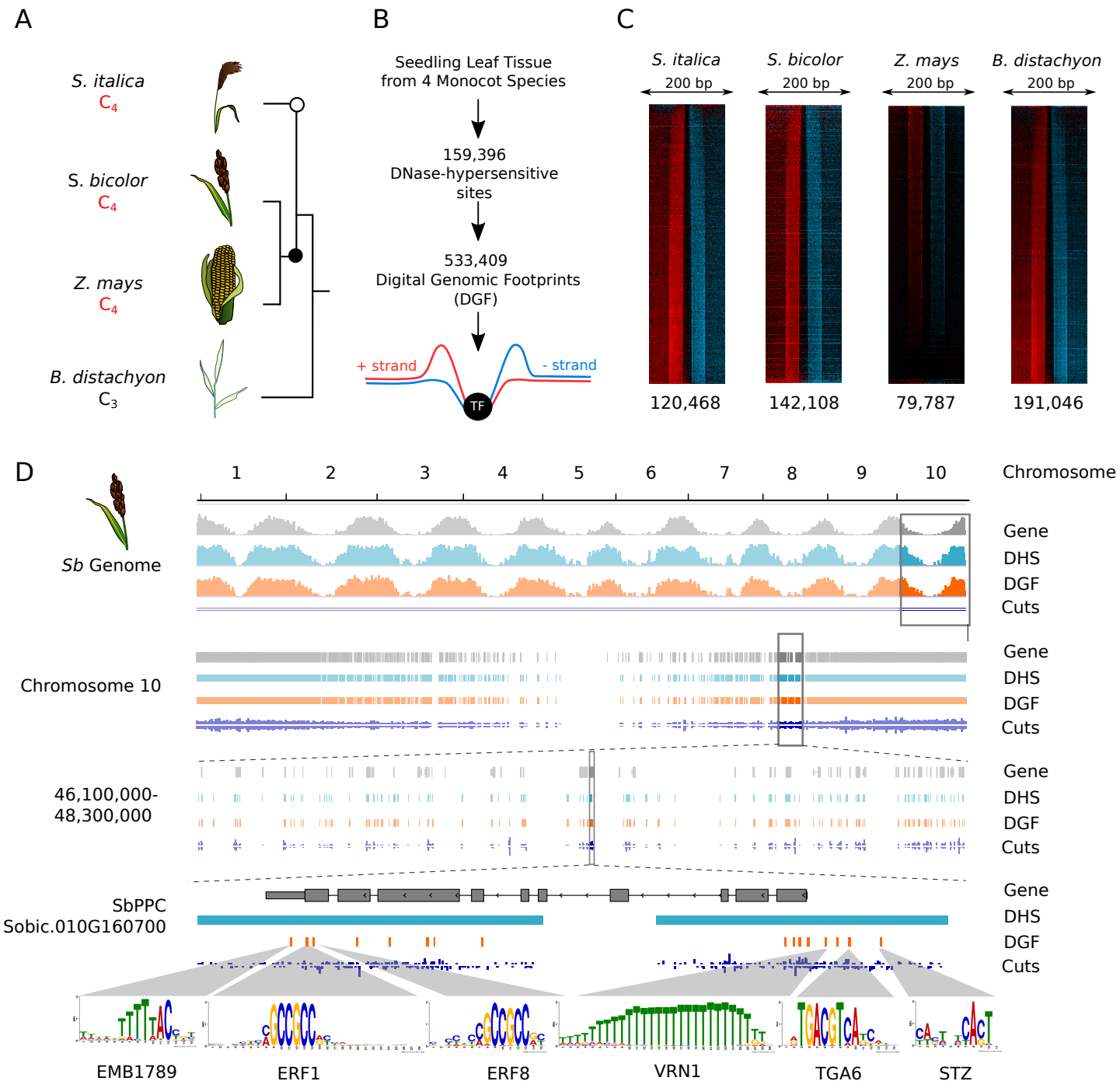
A
S. italica
C4
S. bicolor
C4
Z. mays
C4
B. distachyon
C3
B
Seedling Leaf Tissue
from 4 Monocot Species
159,396
DNase-hypersensitive
sites
533,409
Digital Genomic Footprints
(DGF)
+ strand
- strand
TF
C
S. italica
S. bicolor
Z. mays
B. distachyon
200 bp
120,468
142,108
79,787
191,046
D
Chromosome
Sb Genome
Gene
DHS
DGF
Cuts
Chromosome 10
46,100,000-
48,300,000
SbPPC
Sobic.010G160700
EMB1789
ERF1
ERF8
VRN1
TGA6
STZ

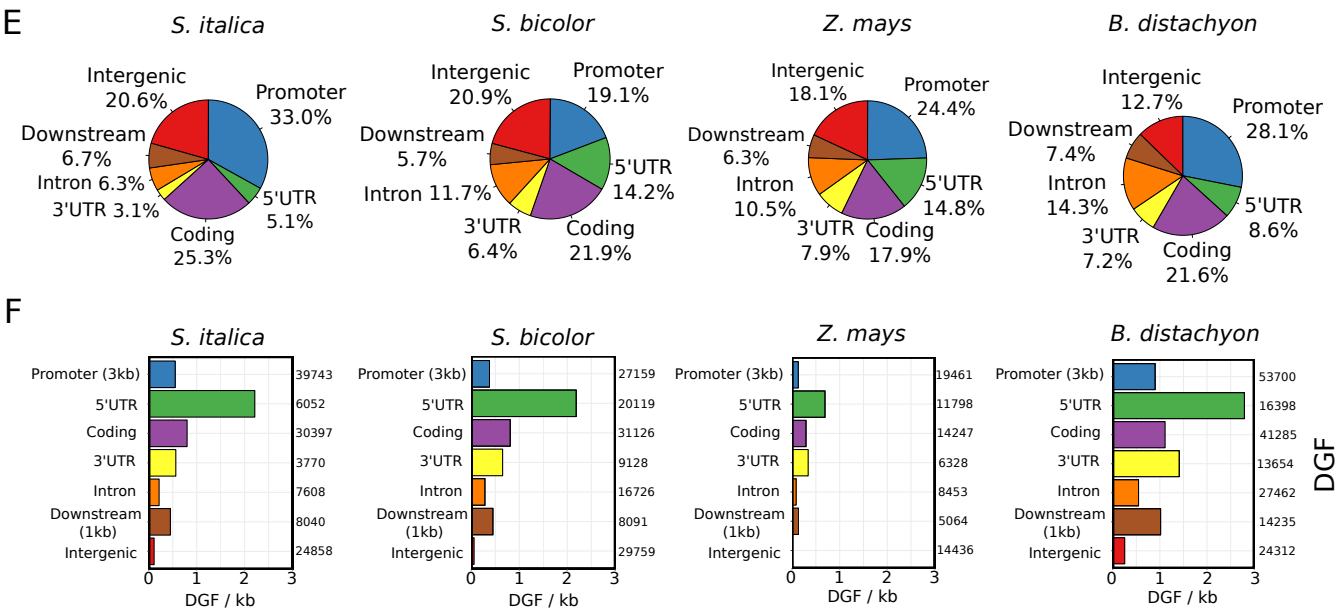
E
S. italica
Intergenic 20.6%
Promoter 33.0%
Downstream 6.7%
Intron 6.3%
3'UTR 3.1%
5'UTR 5.1%
Coding 25.3%
S. bicolor
Intergenic 20.9%
Promoter 19.1%
Downstream 5.7%
Intron 11.7%
5'UTR 14.2%
3'UTR 6.4%
Coding 21.9%
Z. mays
Intergenic 18.1%
Promoter 24.4%
Downstream 6.3%
Intron 10.5%
5'UTR 14.8%
3'UTR 7.9%
Coding 17.9%
B. distachyon
Intergenic 12.7%
Promoter 28.1%
Downstream 7.4%
Intron 14.3%
5'UTR 8.6%
3'UTR 7.2%
Coding 21.6%
F
S. italica
Promoter (3kb) 39743
5'UTR 6052
Coding 30397
3'UTR 3770
Intron 7608
Downstream (1kb) 8040
Intergenic 24858
S. bicolor
Promoter (3kb) 27159
5'UTR 20119
Coding 31126
3'UTR 9128
Intron 16726
Downstream (1kb) 8091
Intergenic 29759
Z. mays
Promoter (3kb) 19461
5'UTR 11798
Coding 14247
3'UTR 6328
Intron 8453
Downstream (1kb) 5064
Intergenic 14436
B. distachyon
Promoter (3kb) 53700
5'UTR 16398
Coding 41285
3'UTR 13654
Intron 27462
Downstream (1kb) 14235
Intergenic 24312
DGF
0 1 2 3
DGF / kb

Figure 1

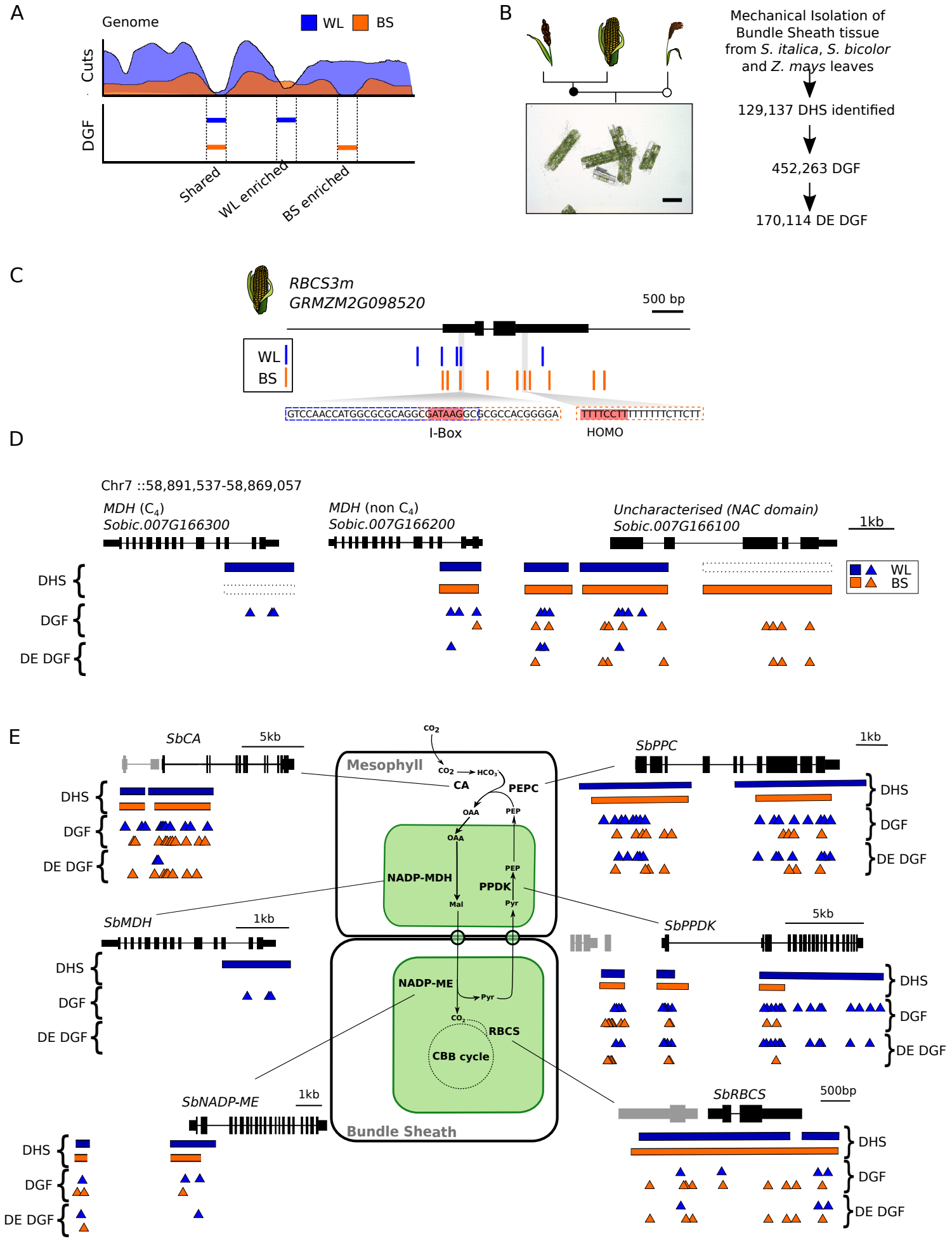
A
Genome
WL
BS
Cuts
DGF
Shared
WL enriched
BS enriched
B
Mechanical Isolation of Bundle Sheath tissue from S. italica, S. bicolor and Z. mays leaves
129,137 DHS identified
452,263 DGF
170,114 DE DGF
C
RBCS3m
GRMZM2G098520
500 bp
WL
BS
GTCCAACCATGGCGCGCAGGCGATAAGGCGCGCCACGGGGA
TTTTCCTTTTTTTTCTTCTT
I-Box
HOMO
D
Chr7 ::58,891,537-58,869,057
MDH (C4)
Sobic.007G166300
MDH (non C4)
Sobic.007G166200
Uncharacterised (NAC domain)
Sobic.007G166100
1kb
DHS
DGF
DE DGF
WL
BS
E
SbCA
5kb
Mesophyll
CO2
CA
PEPC
OAA
PEP
NADP-MDH
PPDK
Mal
Pyr
SbPPC
1kb
SbMDH
1kb
SbPPDK
5kb
NADP-ME
RBCS
CBB cycle
Bundle Sheath
SbNADP-ME
1kb
SbRBCS
500bp
DHS
DGF
DE DGF

Figure 2

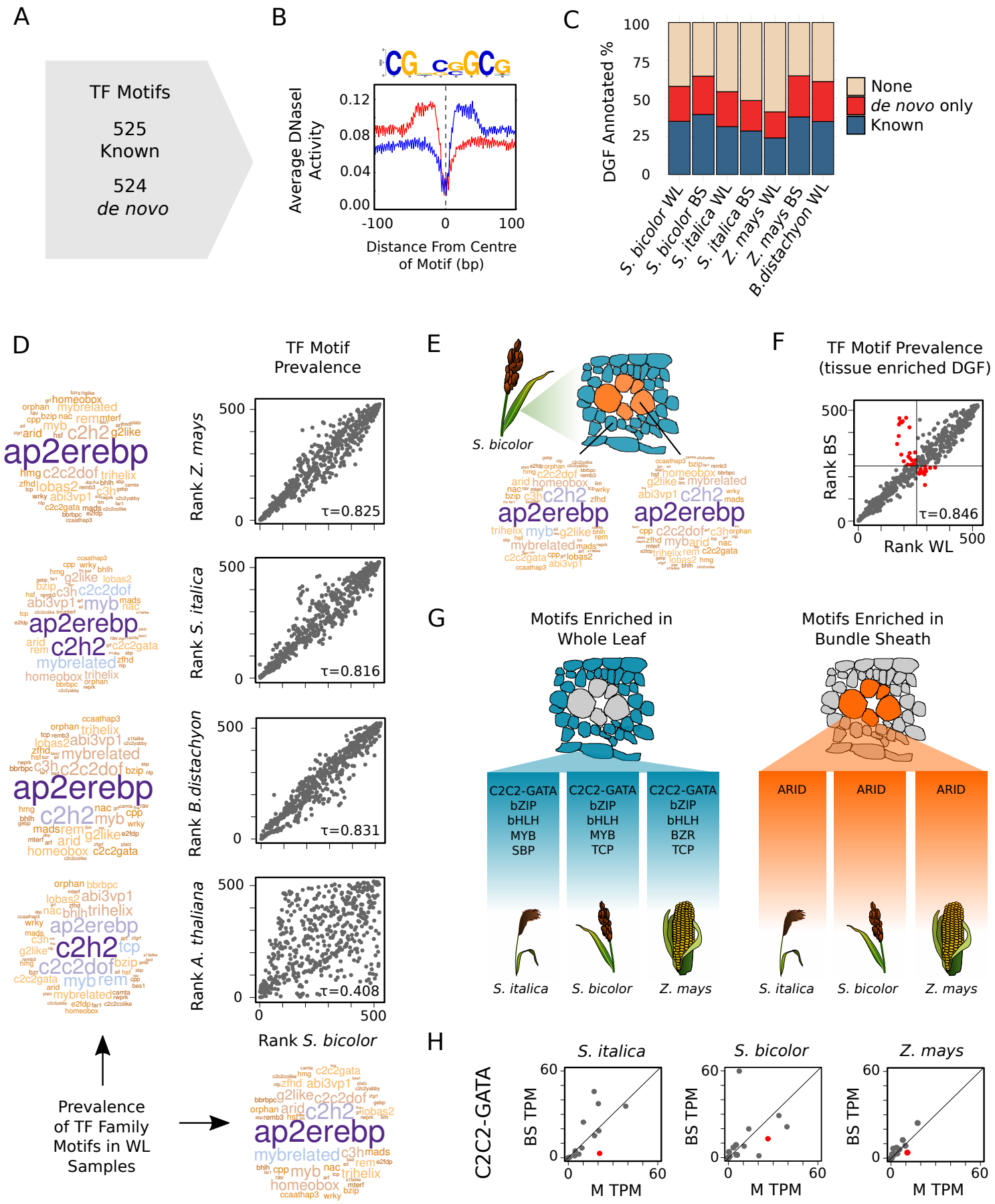
A
TF Motifs
525
Known
524
de novo
B
Average DNaseI Activity
0.12
0.08
0.04
0.00
-100
0
100
Distance From Centre of Motif (bp)
C
DGF Annotated %
100
75
50
25
0
None
de novo only
Known
S. bicolor WL
S. bicolor BS
S. italica WL
S. italica BS
Z. mays WL
Z. mays BS
B.distachyon WL
D
TF Motif Prevalence
Rank Z. mays
τ=0.825
Rank S. italica
τ=0.816
Rank B.distachyon
τ=0.831
Rank A. thaliana
τ=0.408
Rank S. bicolor
Prevalence of TF Family Motifs in WL Samples
E
S. bicolor
F
TF Motif Prevalence (tissue enriched DGF)
Rank BS
Rank WL
τ=0.846
G
Motifs Enriched in Whole Leaf
Motifs Enriched in Bundle Sheath
C2C2-GATA
bZIP
bHLH
MYB
SBP
C2C2-GATA
bZIP
bHLH
MYB
TCP
C2C2-GATA
bZIP
bHLH
BZR
TCP
ARID
ARID
ARID
S. italica
S. bicolor
Z. mays
S. italica
S. bicolor
Z. mays
H
C2C2-GATA
S. italica
S. bicolor
Z. mays
BS TPM
M TPM

Figure 3

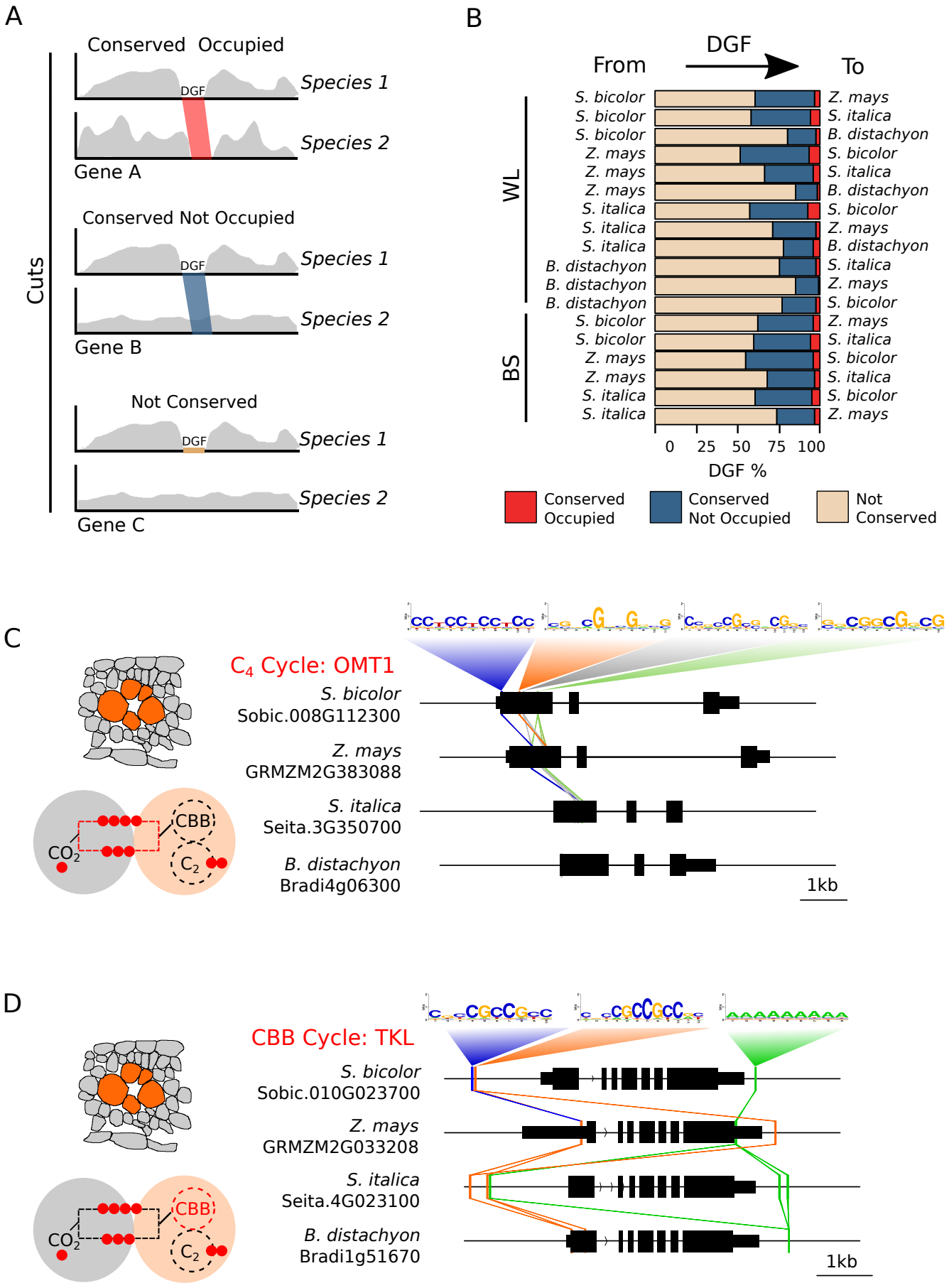
A
Conserved Occupied
DGF
Species 1
Species 2
Gene A
Conserved Not Occupied
DGF
Species 1
Species 2
Gene B
Not Conserved
DGF
Species 1
Species 2
Gene C
Cuts
B
From
DGF
To
WL
BS
S. bicolor
S. bicolor
S. bicolor
Z. mays
Z. mays
Z. mays
S. italica
S. italica
S. italica
B. distachyon
B. distachyon
B. distachyon
S. bicolor
S. bicolor
Z. mays
Z. mays
S. italica
S. italica
Z. mays
S. italica
B. distachyon
S. italica
Z. mays
S. bicolor
Z. mays
S. italica
S. bicolor
S. italica
S. bicolor
Z. mays
0 25 50 75 100
DGF %
Conserved Occupied
Conserved Not Occupied
Not Conserved
C
C4 Cycle: OMT1
S. bicolor
Sobic.008G112300
Z. mays
GRMZM2G383088
S. italica
Seita.3G350700
B. distachyon
Bradi4g06300
1kb
CO2
CBB
C2
D
CBB Cycle: TKL
S. bicolor
Sobic.010G023700
Z. mays
GRMZM2G033208
S. italica
Seita.4G023100
B. distachyon
Bradi1g51670
1kb
CO2
CBB
C2

Figure 4

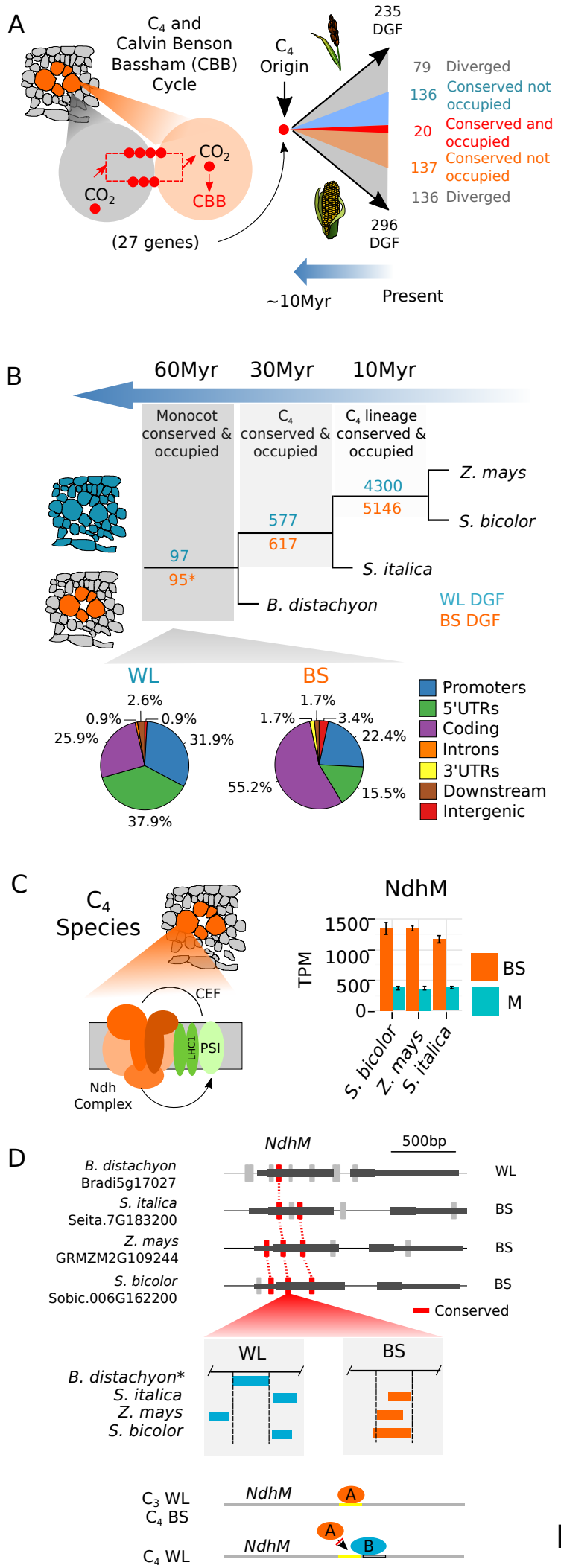
A
C4 and Calvin Benson Bassham (CBB) Cycle
CO2
CO2
CBB
(27 genes)
C4 Origin
235 DGF
296 DGF
79 Diverged
136 Conserved not occupied
20 Conserved and occupied
137 Conserved not occupied
136 Diverged
~10Myr
Present
B
60Myr
30Myr
10Myr
Monocot conserved & occupied
C4 conserved & occupied
C4 lineage conserved & occupied
Z. mays
S. bicolor
S. italica
B. distachyon
4300
5146
577
617
97
95*
WL DGF
BS DGF
WL
BS
2.6%
0.9%
0.9%
25.9%
31.9%
37.9%
1.7%
1.7%
3.4%
22.4%
55.2%
15.5%
Promoters
5'UTRs
Coding
Introns
3'UTRs
Downstream
Intergenic
C
C4 Species
CEF
LHC1
PSI
Ndh Complex
NdhM
TPM
1500
1000
500
0
BS
M
S. bicolor
Z. mays
S. italica
D
NdhM
500bp
B. distachyon Bradi5g17027
S. italica Seita.7G183200
Z. mays GRMZM2G109244
S. bicolor Sobic.006G162200
WL
BS
BS
BS
Conserved
WL
BS
B. distachyon*
S. italica
Z. mays
S. bicolor
C3 WL
C4 BS
NdhM
A
C4 WL
NdhM
A
B

Figure 5